CHALMERS
UNIVERSITY OF TECHNOLOGY

SCIENTIFIC REPORT

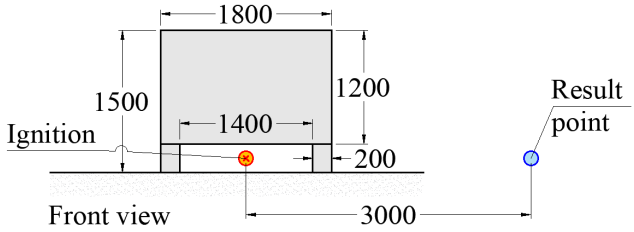

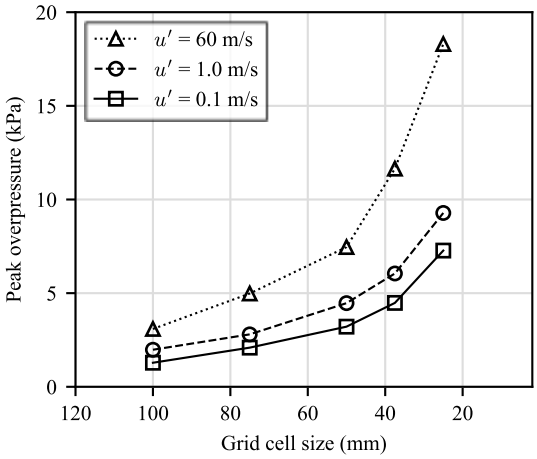

Gas Explosion Simulations in a Traffic Environment

Grid sensitivity analysis and choice of grid resolution

FABIO LOZANO

DEPARTMENT OF ARCHITECTURE AND CIVIL ENGINEERING
Division of Structural Engineering

CHALMERS UNIVERSITY OF TECHNOLOGY
Report ACE 2024:6
Gothenburg, Sweden 2024
www.chalmers.se

REPORT ACE 2024:6

Gas Explosion Simulations in a Traffic Environment

Grid sensitivity analysis and choice of grid resolution

FABIO LOZANO

Department of Architecture and Civil Engineering
Division of Structural Engineering
CHALMERS UNIVERSITY OF TECHNOLOGY
Gothenburg, Sweden 2024

Gas explosion simulations in a traffic environment:
Grid sensitivity analysis and choice of grid resolution
FABIO LOZANO

Report ACE 2024:6
Institutionen för Arkitektur och Samhällsbyggnadsteknik
Chalmers Tekniska Högskola, 2024

Department of Architecture and Civil Engineering
Division of Structural Engineering
Concrete Structures
Chalmers University of Technology
SE-412 96 Gothenburg
Sweden
Telephone + 46 (0)31-772 1000

Cover: Peak overpressure due to an explosion of a propane-air cloud surrounding a personal vehicle calculated with FLACS-CFD v.22. The shown values were obtained at a monitor point located at 3.0 m from the ignition point. The peak overpressure is given as a function of the grid resolution and initial fluctuating velocity.

Gothenburg, Sweden 2024

Gas explosion simulations in a traffic environment:
Grid sensitivity analysis and choice of grid resolution

FABIO LOZANO

Department of Architecture and Civil Engineering
Division of Structural Engineering
Concrete Structures
Chalmers University of Technology

Abstract

Accidental vapour gas explosions in urban environments following an unintended release of a flammable gas during transport could potentially cause great loss of life and resources. Buildings located near roads on which transportation of flammable gas is allowed are subjected to a significant risk for powerful accidental explosions. Furthermore, recent trends for densification of existing urban areas intensify such a risk, which in turn imposes tougher design requirements on the structures exposed to it.

To make a reasonable estimation of the blast load acting on a structure due to an accidental gas explosion, it is essential to properly resolve the explosion scenario itself. Once the strength of the explosion and the amount of energy released is defined, the characteristics of the blast load could be calculated. However, resolving an explosion scenario is no trivial task. Ideally, relevant experimental research would be carried out to investigate the explosion characteristics for the potential accidental scenarios. However, such endeavour would be unfeasible for most practical applications. A more convenient approach, though still challenging, is to use computational fluid dynamics (CFD) codes to numerically solve the equations of compressible flow, turbulence, and combustion.

FLACS-CFD is one of the most used codes in the industry for evaluation of gas explosions. The software relies on the Porosity Distributed Resistance (PDR) method, which utilizes sub-grid models to account for the effect of geometrical elements smaller than the grid cells on small-scale phenomena such as turbulence generation and flame wrinkling. This approach enables the user to discretize the scenario with a coarser mesh, which allows for simulations of large-scale scenarios. However, the presence of sub-grid models in the discretization of the system may introduce significant grid dependency in many cases. As a traditional grid convergence analysis cannot be used for choosing a grid resolution in such cases, the user must follow grid guidelines provided by the developers.

The performance of FLACS-CFD for gas explosions in traffic environment is not thoroughly documented in the literature. Furthermore, grid guidelines may be insufficient for identifying a suitable grid resolution for such an environment. The work presented in this report aims at evaluating the grid dependency of simulations of gas explosions in traffic environment with FLACS-CFD and proposing recommendations for choice of grid cell size based on comparison with published gas explosion experiments.

Keywords: Vapour cloud explosions, FLACS-CFD, overpressure, impulse, grid dependency

Preface

The research work presented in this report is part of a PhD project at the Division of Structural Engineering at Chalmers University of Technology. The PhD project is supervised by Dr Mario Plos, Dr Morgan Johansson and Dr Joosef Leppänen. The study was financially supported by the Swedish Transport Administration (in Swedish: *Trafikverket*), the Swedish Fortifications Agency (in Swedish: *Fortifikationsverket*) and the Swedish Civil Contingencies Agency (in Swedish: *Myndigheten för samhällsskydd och beredskap*).

The work was conducted between February 2021 and December 2023. The PhD project is part of a larger collaboration project between the Division of Structural Engineering at Chalmers and the Division of Concrete Structures at KTH, entitled *Explosions in Densified Urban Environments*, initiated in 2021.

The purpose was to provide practical recommendations for users of the software FLACS-CFD for the choice of grid cell size for simulations of gas explosions consisting of vehicles surrounded by a flammable gas cloud. The outcome of interest of such simulations is the blast load acting on a given point at a certain distance from the explosion centre. This blast load is normally characterized by the overpressure and specific impulse acting on the studied point. This could be relevant, for instance, for the determination of the blast load on the façade of a building located nearby a road where a gas explosion has occurred. The author hopes that this work will contribute towards more consistent and reasonably conservatives results from such simulations, which might translate into similar design conditions for structures affected by blast loads generated by accidental gas explosions.

The calculations presented in this report were performed on two high performance computing (HPC) clusters: *Vera,* managed by the Centre for Computational Science and Engineering (C3SE) at Chalmers University of Technology; and *Tetralith*, managed by The National Supercomputer Centre in Sweden (NSC), an independent centre within Linköping University.

Fabio Lozano

Gothenburg, October 2024

Table of contents

Abstract I
Preface III
Table of contents V
1 Introduction 1
1.1 Background 1
1.2 Aim 2
1.3 Methodology and scientific approach 2
1.4 Limitations 3
1.5 Outline of the report 3
2 Methodology 4
2.1 Overview 4
2.2 Peak overpressure and peak impulse 4
2.3 Gas explosion modelling with FLACS-CFD 6
2.3.1 Description of FLACS-CFD 6
2.3.2 General modelling approach and grid guidelines 6
2.3.3 On the choice of grid resolution 8
2.3.4 On the choice of initial turbulence conditions 8
3 Numerical Campaigns 10
3.1 Overview 10
3.2 Stage I: Campaign I 12
3.2.1 Overview 12
3.2.2 Geometry of the vehicle 13
3.2.3 Monitor points 13
3.2.4 Initial turbulence conditions 13
3.2.5 Ignition 13
3.3 Stage I: Campaign II 14
3.3.1 Overview 14
3.3.2 Monitor points 15
3.3.3 Initial turbulence conditions 16
3.3.4 Ignition 16
3.4 Stage I: Campaign III 16
3.4.1 Overview 16
3.4.2 Geometry 17
3.4.3 Equivalent gas cloud 17

3.4.4 Monitor points 18
3.4.5 Initial conditions 18
3.4.6 Ignition 19
3.5 Stage I: Campaign IV 19
3.5.1 Overview 19
3.5.2 Geometry 19
3.5.3 Monitor points 20
3.5.4 Initial conditions 20
3.5.5 Ignition 20
3.6 Stage II: Campaign V 20
3.6.1 Overview 20
3.6.2 Equivalent gas cloud 22
3.6.3 Result line and monitor points. 22
3.6.4 Initial turbulence conditions 22
3.6.5 Ignition 23
3.6.6 Experimental results 23
3.7 Stage II: Campaign VI 24
3.7.1 Overview 24
3.7.2 Equivalent gas cloud 25
3.7.3 Monitor points 25
3.7.4 Initial conditions 25
3.7.5 Ignition 26
3.7.6 Experimental results 26
4 Results 27
4.1 General 27
4.2 Stage I: Campaign I 27
4.3 Stage I: Campaign II 30
4.4 Stage I: Campaign III 33
4.5 Stage I: Campaign IV 36
4.6 Stage II: Campaign V 38
4.7 Stage II: Campaign VI 40
5 Discussion 42
6 Conclusions 45
References 46

1 Introduction

1.1 Background

Transportation of hazardous materials (hazmat) near or through populated areas is common in our modern society. In general terms, hazmat are materials that have dangerous properties (flammable, explosive, toxic, etc.). In many countries, transportation of hazmat on land in normally carried out by road or railway. Due to the potential catastrophic effects related to accidents involving hazmat, investigation of the consequences of accidents during transportation are of great importance, particularly transportation near urban centres.

An unintended release of a hazmat following an accident during transportation may cause disastrous events such as fires, explosions, and toxic clouds, depending on the characteristics of the released material. A fully develop powerful explosion may result in the greatest losses of life and resources in one single event. Potential sources of explosion commonly transported include flammable gases such as liquified petroleum gas (LPG), liquified natural gas (LNG), and hydrogen. Explosive materials, such as ammunition or fireworks, can also be found in some urban roads; although much less often than flammable gases (Eurostat, n.d.).

An accidental release of a flammable gas can result in different outcomes, depending on the conditions of the accident: jet fires, flash fires, fireballs, and vapour cloud explosions (VCEs). Quantitative risk analyses (QRAs) are carried out to assess the risk associated with an unintended release of a flammable gas in urban environments in connection with transportation of the gas. In simple terms, such an analysis includes the evaluation of the consequences of the potential events following the release and the estimation of the expected frequency of such events. In this process, a VCE is often found to be the most likely event (Bubbico et al., 2000; Casal, 2017). VCEs carry several risk factors with it. Significant damage and injuries may be caused by high temperature, high pressure or flying fragments. Moreover, the explosion gives rise to a blast wave which may cause damage farther away from the explosion centre. Therefore, structures located near roads on which transportation of flammable gases is permitted are exposed to a significant risk for damage caused by accidental VCEs. Densification of existing urban spaces, which may involve building new structures in previously open land next to highly trafficked roads, may increase the severity of such events.

To properly understand the risk associated with VCEs, it is important to perform an accurate estimation of their consequences. This involves estimating the strength of the explosion and the amount of energy released. With that information, the characteristics of the ensuing blast wave may be estimated. Such calculations can be performed with computational fluid dynamics (CFD) codes which numerically solve the equations of compressible flow in combination with turbulence and combustion. Indeed, CFD codes have been used successfully for evaluation of the consequences of gas explosions by different authors e.g., (Middha & Hansen, 2009b; Hansen et al., 2010; Mishra & Mishra, 2021; Shi et al., 2021; Momferatos et al., 2022; Hu et al., 2022).

All CFD codes involve complex physics and numerical schemes, although with different degrees of complexity. In broad terms, CFD codes can be grouped into “simpler” and “advanced” models. Simpler CFD codes, such as EXSIM (B. Hjertager et al., 1996), FLACS-CFD (Gexcon AS, 2022), and PDRFoam (Puttock et al., 2022), implement the Porosity Distributed Approach (PDR) (Patankar & Spalding, 1974) to lessen the need for precise representation of the small-scale geometry, which would impose strict requirements on the calculation grid. Instead, the PDR approach allows to greatly simplify the geometrical conditions by representing sub-grid elements (i.e., objects smaller than the grid cell size) as volume and area porosity and resistance factors. In contrast, more advanced codes attempt to describe the geometry as reliably as possible. Because the PDR approach allows for coarser grids, which enables

simulations of large-scale scenarios, codes based on this approach are used more often for practical applications in the industry.

The inherent disadvantage of the PDR approach is that it requires sub-grid models to account for the effects of objects smaller than the grid. These sub-grid models include a high degree of empirical parameters based on validation of the code against experimental data. Because of this, convergence of the grid is not always possible (Skjold et al., 2014, 2018), and the user must follow grid guidelines provided by the developers. However, the grid guidelines may not cover all possible cases, and the results may depend on the way the user interpret and implement them.

FLACS-CFD is today one of the most used codes based on the PDR approach. Thus, the code carries the drawbacks of the PDR method. Indeed, grid dependency issues have been reported in several research works, e.g., (Makarov et al., 2009; Vyazmina & Jallais, 2016). Attempts at improving the performance of the sub-grid models in FLACS-CFD can be found in the literature (Both et al., 2019). On the other hand, some authors have claimed certain degree of grid independence or, at least, acceptable variation between consecutive grid cell sizes (Hansen et al., 2010; Tolias et al., 2018; Wang et al., 2022). However, this was achieved in scenarios with a high degree of confinement or congestion. For relatively unconfined explosions, such as an explosion on a road or a parking lot, grid dependency continues to be a potential problem.

The use of FLACS-CFD for evaluation of explosions in traffic environments is not thoroughly documented. The reason for this is that FLACS-CFD was originally intended for analysis of gas explosions in settings within the process and chemical industry. Nonetheless, some works dealing with dispersion and/or explosion simulations in traffic environments can be found in the literature, e.g., (Makarov et al., 2009; Middha & Hansen, 2009a; Van den Schoor et al., 2013; Lozano, 2023). Still, much of the published work using FLACS-CFD is concerned with industrial or similar settings. Another issue is that the available grid guidelines may be ambiguous for scenarios consisting of vehicles on a road, which means that the choice of grid cell size may be highly dependent on the personal judgment of the user. All of this indicates that it is necessary to carry out a sensitivity analysis to gain better understanding of the grid dependency in the code for the specific scenario of interest (a gas cloud engulfing vehicles) and, if necessary and possible, to complement the existing grid guidelines with recommendations for choice of a grid cell size for this type of environment.

1.2 Aim

The overall aim of this report is to expand the knowledge about simulations of gas explosions in a traffic environment with the software FLACS-CFD. The environment of interest consists of stationary vehicles inside a flammable hydrocarbon-air mixture with stochiometric concentration. The focus lies primarily on the investigation of the grid dependency of the simulations and potential recommendations for choice of grid cell size that allows for physically reasonable and moderately conservative results.

1.3 Methodology and scientific approach

The work presented in this report consists entirely of numerical analyses with the CFD software FLACS-CFD, version 22. Most of the scenarios analysed are hypothetical scenarios designed to evaluate the performance of different aspects of the software. However, simulations of real experimental research available in the literature were also carried out.

The work was divided into two stages. Each stage was composed of several numerical campaigns. Each campaign contained several scenarios, in which one or several modelling parameters were varied. In Stage I, the focus lay on the grid sensitivity analysis. In Stage II, comparison between experimental results and numerical simulations was carried out.

A complete description of the methodology is provided in Chapter 2.

1.4 Limitations

A summary of the main limitations of the presented work follows below:

- The calculations in this work were carried out with FLACS-CFD, version 22. More recent versions may have a different behaviour regarding grid sensitivity.
- The flammable mixture was modelled as an equivalent gas cloud with a regular shape and uniform stochiometric concentration.
- The vehicles used in the simulations were simplified using rectangular prisms.
- There is not sufficient experimental data concerning gas explosions in the environment of interest available in the literature. Thus, the comparison between simulations and experimental results presented in this report were carried out for experiments of gas explosions between two confinement plates, as an approximation of the flow in the region between the vehicles and the ground.
- The recommendations provided in this report are intended for hydrocarbon gases with low or medium reactivity (e.g., propane) in scenarios in which combustion evolves as a deflagration. Explosions of high-reactivity gases (e.g., hydrogen) or in environments with great potential for a deflagration-to-detonation (DDT) transition are outside of the scope of this work.

1.5 Outline of the report

Chapter 1 presents the background and aim of the report. Moreover, the scope, limitations, a general description of the research methodology are also presented.

Chapter 2 describes the methodology followed to carry out the work, with particular focus on the modelling approach.

Chapter 3 gives a description of the numerical campaigns analysed in this work.

Chapter 4 presents the results of the different numerical campaigns.

Chapter 5 compiles the most relevant outcomes across the different campaigns and presents reflection and discussion about these results.

Chapter 6 summarizes the most important conclusions obtained in this study.

2 Methodology

2.1 Overview

This study seeks to evaluate the grid dependency of gas explosion simulations with the CFD software FLACS-CFD, particularly for scenarios consisting of a vehicle inside a flammable gas cloud with stochiometric concentration. Moreover, the study aims at providing guidance for the choice of grid cell size for simulations in this type of environments that lead to manageable models that produce reasonably conservative results.

The work was divided in two stages. Each stage is composed of several campaigns, which in turn contain several scenarios with varying grid resolution. In some campaigns, other relevant input parameters, such as initial turbulence conditions, were varied between scenarios. The focus of Stage I was on the grid dependency analysis. In Stage II, comparison against experimental work available in the literature was carried out to identify suitable grid resolutions for the environment of interest. A complete description of the numerical campaigns is provided in Chapter 3.

To facilitate the comparison between multiple scenarios, each generating a large amount of data, the study was limited to the results at a few selected monitor points or result paths. The parameters compared were the peak overpressure and the peak impulse, as defined in Section 2.2.

A general description of the general approach followed to create the CFD models, as well as a brief description of the known challenges regarding grid generation and initial turbulence conditions with FLACS-CFD is given in Section 2.3.

The calculations were performed in FLACS-CFD, version v.22, on two high performance computing (HPC) clusters: *Vera*, by C3SE, centre for scientific and technical computing at Chalmers University of Technology; and *Tetralith*, by The National Supercomputer Centre in Sweden (NSC).

2.2 Peak overpressure and peak impulse

When a fuel-air mixture explodes, the combustion products rapidly expand to a volume much larger than the unburned volume. That is, the chemical energy stored in the fuel-air mixture is released and converted into mechanical energy. This mechanical energy is transferred to the surrounding air particles which are pushed away from the centre of the explosion as a blast wave (Johansson, 2012). At a given point at a certain distance from the explosion centre, the passage of the blast wave is experienced as a transient, often quick, change in thermodynamic state, defined by parameters such as pressure, density, and temperature (Center for Chemical Process Safety, 2010). Within the context of blast-resistant design, it is common to characterize the blast wave based on its pressure-time history, usually defined with the help of the so-called blast wave parameters. The different blast waves parameters are described for an ideal blast wave in Figure 1. The parameter ΔP is the overpressure, which is defined as $\Delta P = P - P_0$. Here, P is the absolute pressure and P_0 is the ambient pressure (approx. 102 kPa at 15° C). The parameter ΔP^+ represents the peak overpressure; that is, the greatest overpressure registered at the studied point. The use of overpressure is preferred because any damage in a blast-loaded structure will be caused by the pressure relative to the ambient pressure.

It should be noted that the shape of the pressure-time history in the free field depends mainly on the amount of energy released by the explosion, the speed of the release, and the distance from the explosion centre. The shape presented in Figure 1 is a schematic representation of an ideal wave in free-field conditions. However, in more complex environments with obstruction or confinement, the shape may look different, and several peaks may be observed. An example is given in Figure 2a), taken from a scenario with two-dimensional confinement (see Campaign V in Chapter 3). In this example, the peak overpressure is around 14 kPa at $t = 0.060$ s, but a secondary peak can be discerned at around $t = 0.065$ s. Due to the deviation of the overpressure-time history from the ideal representation, it may not be suitable

or desirable to directly compare the pressure-time history of different numerical scenarios. Instead, the comparison can be made for two specific parameters: peak overpressure and peak impulse. The impulse[1] is defined as the integral of the overpressure-time history. The peak impulse is the maximum positive impulse during the simulation time. For a simple shape as the one given in Figure 1, the parameter i^+ could be used directly. However, when there are several positive overpressure peaks, mixed with short periods of negative overpressure, it is more convenient to utilize the peak impulse. In Figure 2b), an example of the variation of the impulse with time is given. The peak impulse for this case occurs at about $t = 0.07$ s and has a magnitude of around 105 Pas.

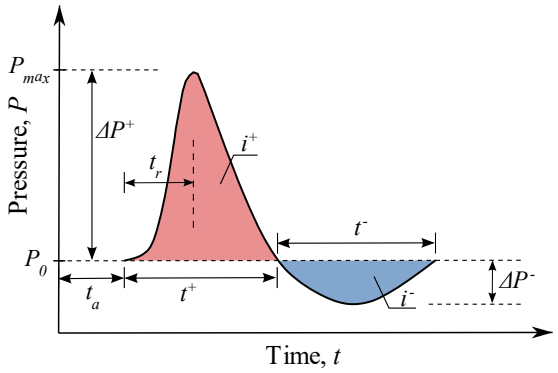

ΔP^+: Peak overpressure
ΔP^-: Peak underpressure
i^+: Positive specific impulse
i^-: Negative specific impulse
t^+: Duration of positive phase
t^-: Duration of negative phase
t_a: Time of arrival
t_r: Rise time

Figure 1. Definition of blast wave parameters. Taken from (Lozano, 2023). The red shaded area corresponds to the positive phase, while the blue shaded area corresponds to the negative phase.

a) Overpressure vs time

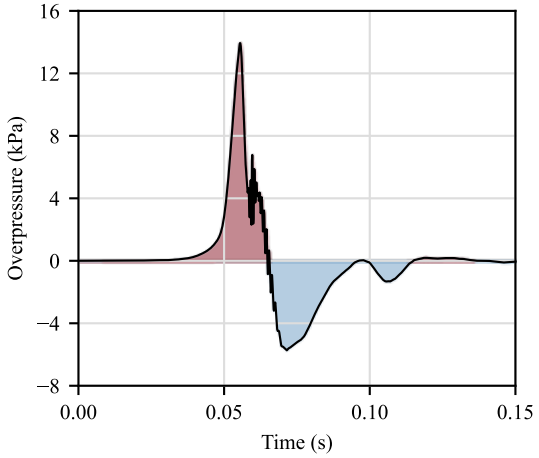

b) Impulse vs time

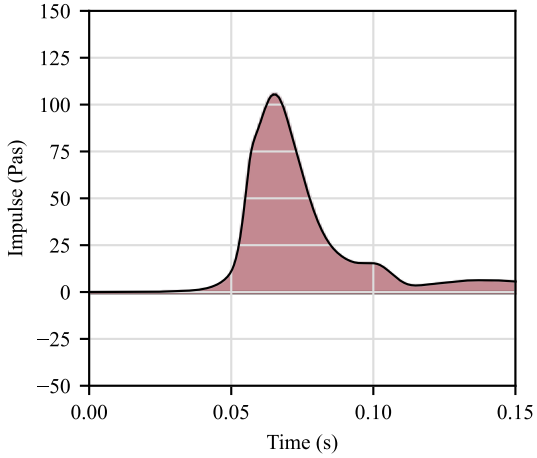

Figure 2. Example of a) the overpressure-time history and b) the impulse-time history at a point outside a confined obstructed region (see Campaign V in Chapter 4). The red shaded area corresponds to the positive phase.

In this report, the comparison between different models with different grid resolutions is made mostly based on the peak overpressure and the peak impulse. Furthermore, only the positive phase is considered in the comparison.

[1] When the impulse is calculated as the integral of the overpressure-time history, it has dimensions of pressure-time product. For this case, the term *specific impulse* is more appropriate. However, several authors use simply *impulse* within the context of blast-loading if there is no ground for confusion. Therefore, the term *impulse* is used throughout all this document as a simplification of *specific impulse*.

2.3 Gas explosion modelling with FLACS-CFD

2.3.1 Description of FLACS-CFD

FLACS-CFD utilizes the finite volume approach to solve the Navier-Stokes equations for compressible flow in conjunction with combustion and turbulence on a structured cartesian grid (Gexcon AS, 2022). The governing equations that are simultaneously solved by the code comprise conservation of mass, momentum and energy, transport of fuel mass fraction and mixture fraction, turbulent kinetic energy, and rate of dissipation of turbulent kinetic energy. A thorough description of the background of FLACS-CFD can be found in e.g., (B. H. Hjertager, 1984, 1993; Arntzen, 1998).

FLACS-CFD uses the Porosity Distributed Resistance (PDR) approach to achieve a solution regarding combustion and turbulence with a relatively coarse grid. This approach was initially proposed by (Patankar & Spalding, 1974) and further developed in e.g., (Sha & Launder, 1979; Sha et al., 1982). According to the PDR approach, sub-grid elements (i.e., objects which are smaller than the grid cells) are numerically represented by a volume and area porosity value ranging from 0 (fully obstructed) to 1 (fully open) and resistance factors at each grid cell. Several sub-grid models involving empirically determined parameters are used in the discretization of the governing equations, which enables consideration of, for example, the effects of sub-grid objects on turbulence generation and flame wrinkling using a simple cartesian grid. This allows to software to bypass the need for resolving small objects with small grid cells.

Turbulence is incorporated based on the well-known k-ε turbulence model (Launder & Spalding, 1974). Closure of the turbulence model is achieved with sub-grid models for turbulence generation due to sub-grid objects. Combustion is handled in FLACS-CFD as an irreversible reaction process with a finite reaction rate (B. H. Hjertager, 1984). This combustion model has three essential components: a flame model, a burning velocity model, and a flame-folding model. The flame model was developed based on the research in (Arntzen, 1998). The burning velocity model correlates the burning velocity with the properties of the mixture and the flow regime (which can be laminar, quasi-laminar, or turbulent) with the help of a series of empirically determined equations. Lastly, the flame-folding model accounts for the increase in burning rate due to folding of the flame around the sub-grid obstacles.

2.3.2 General modelling approach and grid guidelines

The user of FLACS-CFD must rely on strict grid guidelines to achieve acceptable predictions of gas explosions scenarios with the software. The guidelines are provided in the user's manual for FLACS-CFD (Gexcon AS, 2022). The guidelines were formulated based on validation of the software against experimental data. Following the guidelines ensures that the empirical parameters in the theoretical formulations are used within the conditions for which they were calibrated and/or validated. Over the years, the grid guidelines in FLACS-CFD have been updated to account for new developments in the code. For example, in the first commercially available version of FLACS-CFD, the grid could only have a constant cell size of 1.0 m, while later versions allowed for some variations of the grid cell size (Lea & Ledin, 2002). Recommendations for minimum cell size and maximum cell size are also updated regularly. For instance, in v.22 the minimum allowed cell size is 10 mm (Gexcon AS, 2022), while in v.21 the minimum allowed cell size was 15 mm (Gexcon AS, 2021).

In accordance with the grid guidelines in v.22, the following actions were implemented in all simulations performed in this study, unless specified otherwise in the description of the numerical campaigns in Chapter 3:

- The calculation domain was divided into a *core domain* and a *stretched domain.* Only results from the core domain are accepted. The stretched domain is a buffer zone between the core domain and the boundary conditions intended to minimize the potential influence of the boundary conditions on the results inside the core domain. Results from the stretched domain are therefore disregarded. Figure 3 shows a schematic description of the calculation domain.

- In the core domain, the grid consisted of cubical cells with constant size. In the stretched domain, the cell size was gradually stretched with a geometrical progression (with a factor of 1.2).
- The unburned gas cloud and all objects within the cloud were modelled entirely inside the core domain.
- The core domain was chosen large enough to prevent the flame from travelling into the stretched domain.
- The minimum allowed grid cell size was set to 10 mm overall.
- The Courant-Friedrich-Levy numbers, CFLC and CFLV, were set to the default values: 5 and 0.5, respectively.
- The option STEP = "KEEP_LOW" was used. This guarantees sufficiently short time steps even when most of the fuel has burned, which prevents numerical damping of the pressure waves in later stages of the simulation.
- Non-reflecting boundary conditions (known as PLANE_WAVE in FLACS-CFD) were used at all boundaries apart from the ground. EULER boundary condition was used on the ground.

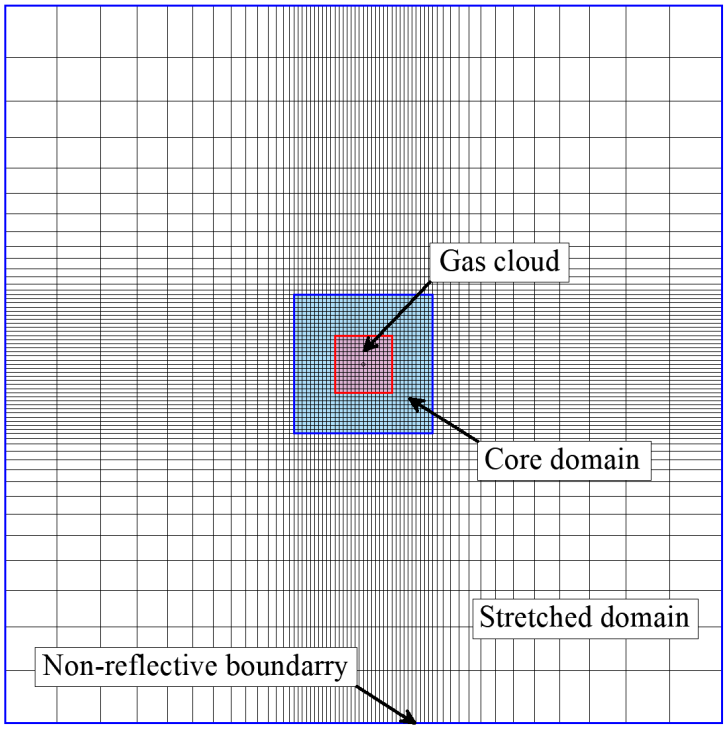

Figure 3. Schematic description of the calculation domain and grid layout. The figure shows a plan view. The grid cell has a constant size within the core domain.

All objects present in the calculation domain were assumed to be fixed and rigid during the simulations. For most scenarios with vehicles, all edges of the geometry were aligned with the grid. In a few scenarios with vehicles, in which the grid cell size was not a divisor of all the dimensions of the vehicle, alignment between the grid and the geometry was optimized as much as possible. For scenarios in which congestion was produced by tubes, it was not possible to model all geometrical shapes on the grid. For such cases, the geometry of the tubes and their effects were handled by the PDR approach. Lastly, when confining plates were present in the simulation, their geometry was entirely resolved on a grid plane.

2.3.3 On the choice of grid resolution

The choice of grid resolution according to the grid guidelines is by and large based on the minimum cloud extent. The advantage of this approach is that it allows the developers to provide general recommendations that could be implemented in different scenarios, regardless of the scale. In v.22 (Gexcon AS, 2022), the maximum allowed cell size is calculated as $D/15$, where D is the minimum cloud extent. That is, the cloud should have at least 15 cells along its smallest dimension. The exact definition of cloud extent has varied over different versions of the software. In v.22, the minimum cloud extent corresponds to the minimum dimension of the cloud. In v.20 (Gexcon AS, 2020), the minimum cloud extent should also account for the dimension of regions of high congestion and confinement within the cloud, besides the dimensions of the cloud itself. According to this definition, the minimum cloud extent for unconfined clouds is the minimum dimension of the cloud. However, for confined clouds, the minimum cloud extend may be given by the main dimension of confinement inside the cloud.

Besides discretization of the minimum cloud extent, the choice of grid cell size should also account for other parameters within the domain, such as minimum cell count across vents, minimum cell counts between the core domain and the boundary conditions, and minimum cell count outside vents. The specific recommendations for the different details may vary from one version to the next.

Intuition dictates that for scenarios dominated by congestion or confinement, the choice of the cell size should be based not only on the dimensions of the cloud but also on the minimum dimension of congestion or confinement. This means that for scenarios in which confinement between two planes covers a significant volume of the cloud and combustion and expansion is predominantly two-dimensional, the distance between the two confinement planes would determine the minimum cloud extent. However, for some cases, the dimension in the direction of confinement may be relatively small, and it may not be reasonable to follow the rule about maximum cell size (i.e., $D/15$), as this would produce unreasonably small grid cells, which may even be smaller than the minimum allowed grid cell size. Furthermore, for cases in which the volume of the confined region is relatively small in relation to the total gas volume (e.g., the region under a vehicle compared to the total gas volume engulfing a vehicle), it is unclear if the cloud extent should be based on the cloud dimensions or on the confining geometry.

For cases in which ambiguity exists among the grid guideless, some degree of engineering judgment is required, and care should be taken to ensure that the geometry and the flow is resolved properly in this region. For such cases, the user's manual recommends a sensitivity study to ensure that the grid dependency is not too high.

Consequently, it may not be possible to find an appropriate and consistent cell size for scenarios involving a vehicle engulfed by a gas cloud by following the grid guidelines. Two different users may choose different grid cell sizes, which could lead to significantly different outcomes. Furthermore, confinement in the space under the cars is likely to play a significant role in the resulting explosion and properly resolving this region is of upmost importance in such a simulation. Therefore, a grid convergence analysis is required to investigate the influence of the cell size and to find a suitable grid cell size.

2.3.4 On the choice of initial turbulence conditions

Another important challenge in setting up the model is the definition of the initial turbulence conditions. The user's manual explains that the initial turbulence will likely have little effect for simulations with a strong geometrical congestion, since turbulence will be generated rapidly by the geometry inside the explosion soon after combustion starts. However, for scenarios with little congestion near the ignition point, the initial turbulence conditions should be defined properly as it could influence the results markedly. The initial turbulence conditions are described by the isotropic fluctuating velocity, u', and the turbulence length scale (l_{LT}). The isotropic fluctuating velocity is defined as the product of the characteristic velocity (U_0), which is the reference mean flow velocity, and the relative turbulence intensity (I_T), which gives the level of turbulence. The fluctuating velocity is used to calculate the turbulent kinetic energy (k) at the beginning of the simulation, while the turbulence length scale is used to calculate the dissipation rate of the turbulent kinetic energy (ε) at the beginning of the simulation.

The default value of the initial fluctuating velocity in FLACS-CFD is 200 m/s × 0.3 = 60 m/s, which corresponds to an estimate of the mean flow velocity of a jet release with a high turbulence intensity. The author believes that these values are too conservative for gas explosions in traffic environments, and more appropriate initial values must be found for gas explosion scenarios in such environments. However, there is little information regarding the treatment of these factors in simulations with FLACS-CFD in the literature.

Though information concerning initial turbulence conditions is often not reported in research articles in which FLACS-CFD was used, a few noteworthy cases can be found. (Mishra & Mishra, 2021) carried out a numerical study of a large-scale unconfined LNG VCE using FLACS-CFD. The characteristic velocity in that study was set to 2 m/s based on the expected wind speed. The relative turbulence intensity was set to 0.1. This led to an initial fluctuating velocity of 0.2 m/s. In (Vyazmina & Jallais, 2016) and (Pedersen & Middha, 2012), an initial fluctuating velocity of 0.1 m/s was used for simulating vented hydrogen explosion. Here, measurements of initial fluctuating velocity from experiments were available for one of the simulated cases.

The turbulence length scale (l_{LT}) is easier to treat as it depends on the grid cell size. According to the user's manual, the turbulence length scale should not be set higher than the default value (0.05 m) or 50 % of the cell size.

The initial turbulence conditions introduce uncertainties into the simulations since it can significantly affect the rate of combustion. For that reason, a sensitivity study must be carried out to evaluate the effect of adjusting the initial turbulence conditions and to find reasonable values for the cases at hand.

3 Numerical Campaigns

3.1 Overview

The work compiled in this report consists of a series of numerical campaigns grouped into two different stages. A brief description of these campaigns is presented in Table 1. Within each campaign, several scenarios were analysed. In total, 106 scenarios were simulated.

The main objective of Stage I was to investigate the grid dependency of numerical analyses of explosion of a mixture of a flammable hydrocarbon gas and air (referred to simply as a gas cloud) with the CFD software FLACS-CFD. The main gas of interest in the study was propane, although simulations of scenarios with ethylene were also carried out. In all analyses, the gas cloud was assumed to have a uniform stochiometric concentration and to be shaped as a rectangular cuboid. The study focused on an environment consisting of a vehicle engulfed by a stochiometric gas cloud. The geometry of the vehicles in the different campaigns was simplified in the numerical models. Both the body and wheels were built up using rectangular cuboids. However, grid dependency was also investigated for other geometrical conditions in which the main source of obstruction consisted of repeating cylindrical obstacles. Furthermore, the impact of the initial turbulence conditions as well as the effect of the grid size in relation to the height of the gas cloud and confinement was studied.

Table 1. Summary of the numerical campaigns.

	Campaign	No. scenarios	Description
STAGE I	I	12	This campaign studied both unconfined explosions as wells as explosions in scenarios with a vehicle inside the cloud. The gas cloud consisted of a cubic stochiometric propane-air cloud with size of 6.0 m.
	II	23	This campaign studied simulations of the gas explosion experiments in a 27-m^3 corner by (B. Hjertager et al., 1988). Here, grid dependency was studied in relation to volume blockage ratio (*VBR*) and obstacle diameter (*D*).
	III	25	In this campaign, explosion simulations of stochiometric propane-air clouds surrounding one vehicle were carried oud. The focus of the campaign was grid dependency in relation to the height of the gas cloud.
	IV	15	This campaign performed explosion simulations of a gas cloud surrounding one vehicle. The cloud consisted of a stochiometric propane-air cloud with size 6.8×3.8×1.8 m. The effect of the initial turbulence conditions was investigated.
STAGE II	V	23	Simulations of the gas explosion experiment by (van Wingerden, 1984) were carried out. The experiment focused on two-dimensional expansion between two confining plates. Congestion was introduced by horizontal tubes between the plates. The aim of this campaign was to find a suitable grid cell size for simulation of explosions of a gas cloud within two-dimensional confinement.
	VI	8	Simulations of the gas explosion experiment in (van Wingerden, 1989) were carried out. The experiment focused on two-dimensional expansion between confining plates. The obstruction was produced by short vertical pipes between the plates. The aim of this campaign was to test the guidance for choice of grid cell size from campaign V.

The default value of the initial fluctuating velocity in FLACS-CFD is u' = 60 m/s. This corresponds to an estimate of the mean flow velocity of a jet release with high turbulence intensity. This default setting was used for most simulations. However, the effect of the initial fluctuating velocity was investigated in some of the campaigns in conjunction with the grid sensitivity analysis. In such campaign, two other values, besides the default value, were tested. The additional values for u' were 0.1 m/s and 1.0 m/s. The lowest value was calculated based on a "mild" wind speed of 1 m/s and a relative turbulence intensity of 0.1. The second value was based on a "high" wind speed of 10 m/s and relative turbulence intensity of 0.1. This second value is considered a realistic upper limit of the initial turbulence conditions for the environment in a city road.

In Stage II, the study focused on identifying an appropriate grid cell size for situations dominated by two-dimensional flame expansion. The reason for focusing on two-dimensional confinement was that combustion in the space under a group of vehicles (where the flow is mainly two-dimensional) is the most likely source of strong blast in the event of ignition of a gas cloud on a road, if the vehicles themselves are the only source of confinement or congestion. The choice of grid cell size was achieved through comparison between experimental results and simulations of gas explosion experiments available in the literature. The criteria for selecting relevant experiments for this comparison included:

- The expansion of flame and gases should be primarily two-dimensional, preferably through a congested region.
- The experimental set-up should be well-defined to decrease the uncertainty in the modelling process.
- The ignited mixture should preferably consist of air and propane or another gas with similar properties.
- Experimental results (such as overpressure and flame speed), both inside and outside the confined area, should be available, preferably at different points, to facilitate comparison between the numerical analyses and experiments.

Two experiments were chosen for the evaluation in Stage II. The first experiment (see Campaign V) consists of a study of the deflagration of an ethylene-air mixture in a congested region confined between two planes as described in (van Wingerden, 1984). In this experiment, congestion was introduced with the help of parallel *horizontal* tubes. Besides the effects of the obstacles on flame propagation, the influence of the distance between planes and the porosity of the top plate was evaluated in this study. Available results include values of flame speed inside the confined region and peak overpressure outside the confined region. The second experiment studied (see Campaign VI), which is often referred to as DISCOE, also deals with deflagrations between two parallel planes, but with obstacles in the form of *vertical* tubes in a radial arrangement (van Wingerden, 1989). The effects of pitch, confinement, gas reactivity, and distance between congested regions were studied. From this experiment, values of flame speed inside the confined region are available for different gases, including ethylene and propane. The first experiment was chosen as the basis for the choice of grid cell size, as results for both flame velocity and overpressure both inside and outside the confined region are available. The DISCOE experiment was later used to test the conclusions reached from the comparison with the first experiment.

In the following sections, a general description of the different campaigns is provided, including the geometry, characteristics of the gas cloud, location of monitor points, and compilation of the different configurations and scenarios within a given campaign. Unless specified otherwise, the general approach described in Section 2.3 was followed to create the numerical models of the scenarios.

Here, the cell size is also reported in terms of N, which is the number of cells along the smallest cloud dimension. The cell size is treated in this manner since the grid guidelines in the user's manuals are given in terms of number of cells for different situations.

3.2 Stage I: Campaign I

3.2.1 Overview

In this campaign, simulations of a hypothetical explosion of a propane-air cloud were carried out for different grid cell sizes and obstruction conditions. The cloud was assumed to have a uniform stochiometric concentration (equivalence ratio[2] of 1.05[3]). The cloud had a cubic shape with side 6.0 m. In half of the scenarios, no obstacle was present within the cloud (configuration 1). That is, the cloud was completely unobstructed and unconfined on all sides apart from the ground, see Figure 4a). In the remaining scenarios, a mock-up vehicle was introduced inside the cloud (configuration 2), as shown in Figure 4b).

a) Unconfined/unobstructed scenario *b*) Scenario with a vehicle

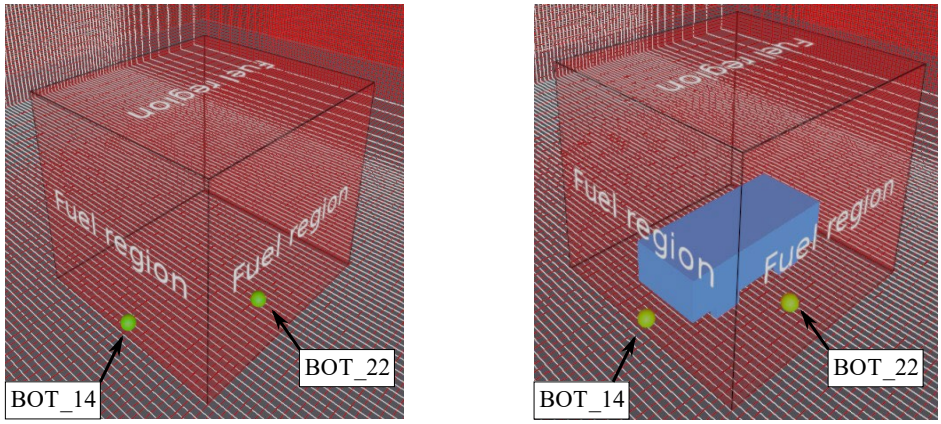

Figure 4. Equivalent gas cloud and relevant monitor points in Campaign I.

Several grid cell sizes were studied. The coarsest cell size corresponds to 15 elements along the height of the cloud (6.0 m/15 = 400 mm), while the finest cell size is given by 120 elements along the height of the cloud (6.0 m/120 = 50 mm). A total of 12 scenarios, divided into two configurations, was analysed, as presented in Table 2.

Table 2. Summary of studied scenarios and corresponding cell sizes within Campaign I.

Campaign	Configuration	Scenario	Vehicle	Cloud height [mm]	Cell size, h [mm]	No. cells along cloud height, N
I	1	1	No	6000	400	15
I	1	2	No	6000	200	30
I	1	3	No	6000	150	40
I	1	4	No	6000	100	60
I	1	5	No	6000	80	75
I	1	6	No	6000	50	120
I	2	7	yes	6000	400	15
I	2	8	yes	6000	200	30
I	2	9	yes	6000	150	40
I	2	10	yes	6000	100	60
I	2	11	yes	6000	80	75
I	2	12	yes	6000	50	120

[2] The equivalence ratio is as measure of the concentration relative to the stochiometric concentration of the mixture. An equivalence ratio of 1.0 means that the mixture has a stochiometric concentration, while a value greater than 1.0 means that the actual concentration is higher than stochiometric.

[3] The laminar burning velocity (which relates to the explosion potential) for hydrocarbon fuels is greatest at a concentration slightly above the stochiometric concentration. For propane, this occurs at around an equivalent ratio of 1.05 (Bradley, 1978).

3.2.2 Geometry of the vehicle

The mock-up vehicle was modelled with a simplified geometry as depicted in Figure 5. The body of the vehicle was assumed to be a rectangular prism with dimensions 4.8×2.0×1.2 m. The wheels were modelled as rectangular prisms with dimensions 0.8×0.2×0.4 m. All dimensions are multiple of 50 mm and 20 mm, which facilitated aligning the grid to the geometry of the vehicle.

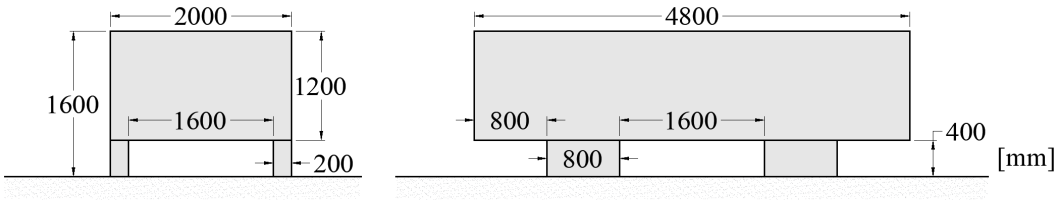

Figure 5. Geometry of mock-up vehicle in Campaign I.

3.2.3 Monitor points

A total of 14 monitor points were created to collect results from the simulation. In this report, results are only presented at two monitor points: BOT_14, and BOT_22, see Figure 6. BOT_14 is placed at 3.0 m from the ignition point in the direction parallel to the vehicle (around 0.5 m from the edge of the vehicle). BOT_22 is placed at 2.0 m from the ignition point in the direction perpendicular to the vehicle (around 1.0 m from the edge of the vehicle). The points are placed at an elevation of 0.2 m above the ground.

Side view: Front view:

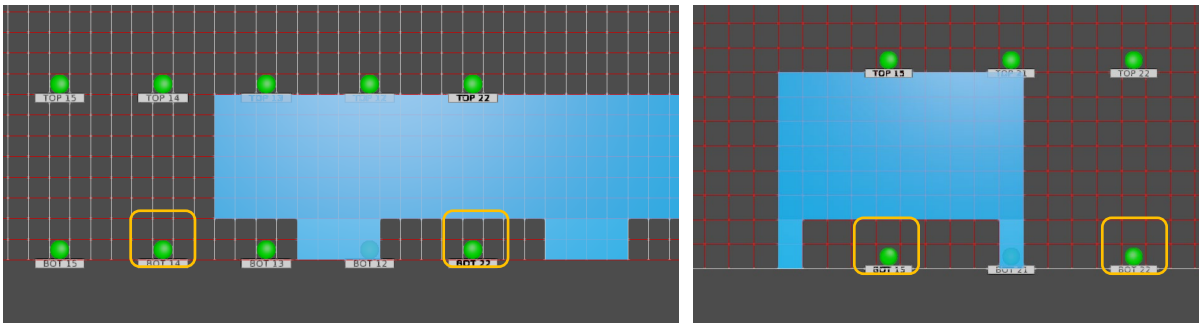

Figure 6. Monitor points in relation to the vehicle in Campaign I.

3.2.4 Initial turbulence conditions

The default initial conditions were used in this campaign, as defined below:

- Characteristic velocity: 200 m/s
- Relative turbulence intensity: 0.3
- Turbulence length scale: 0.05 m

3.2.5 Ignition

The ignition point was nominally placed in the space between the vehicle and the ground at the centre of the confined region and at an elevation of 0.2 m. However, the final position of the ignition point was adjusted to the closest cell centre for the different grid cell sizes. The impact of this small shift in the position of the ignition point is deemed to be negligible.

3.3 Stage I: Campaign II

3.3.1 Overview

This campaign consisted of simulations of an experimental research of spherical flame propagation in a region with high-density obstruction. The complete description of the experimental setup and results can be found in (B. Hjertager et al., 1988). The vessel was shaped as a corner with two vertical walls and a ground plate, see Figure 7. The dimensions of the vessel are 3×3×3 m, which results in a volume of 27 m^3. Obstruction was introduced into the vessel in the form of horizontal pipes arranged in a grid pattern with multiple horizontal layers, see Figure 8. Both the diameter of the pipes and the number of pipes were varied to create multiple scenarios with different volume blockage ratios (*VBR*). In the experiments, explosions of methane-air and propane-air mixtures were studied. However, in this report, only explosions of propane-air (equivalence ratio of 1.05) were analysed. The equivalent cloud is assumed to have filled the entire vessel, that is, the cloud was assumed to have dimensions 3×3×3 m. This experiment was included in this study as a representative environment suitable for implementation of the PDR approach. The different configurations and scenarios analysed in this study are given in Table 3.

In FLACS-CFD, the obstacles were modelled as solid cylinders with length 3.0 m and variable diameter, while the walls and ground were modelled as rigid surfaces. The modelled geometry for the different configurations is depicted in Figure 9.

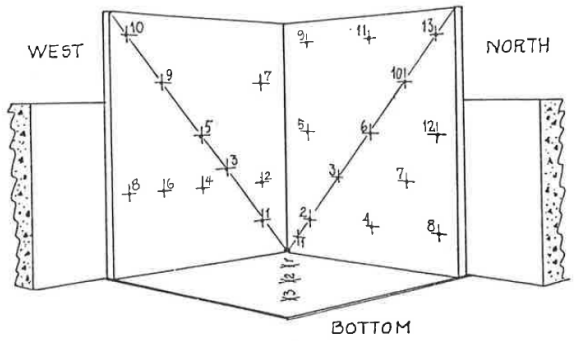

Figure 7. Schematic vie of the 27-m^3 in (B. Hjertager et al., 1988).

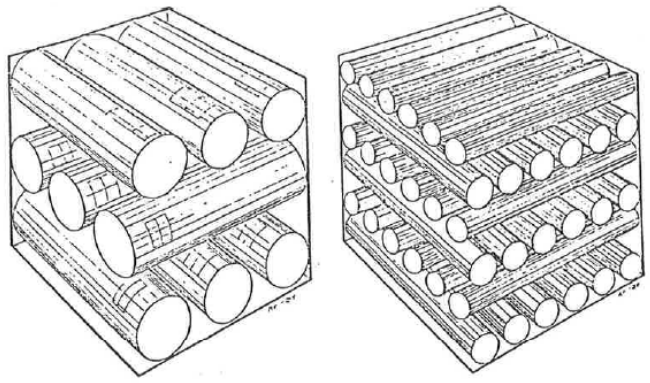

Figure 8. Two examples of different obstacle densities in (B. Hjertager et al., 1988).

Table 3. Summary of studied scenarios and corresponding cell sizes within Campaign II.

Campaign	Configuration	Scenario	*VBR*	*D* [mm]	Cell size, *h* [mm]	No. cells along cloud height, *N*
II	1	1	0.2	410	400	7.5
II	1	2	0.2	410	300	10.0
II	1	3	0.2	410	200	15.0
II	1	4	0.2	410	180	16.7
II	1	5	0.2	410	150	20.0
II	1	6	0.2	410	130	23.1
II	1	7	0.2	410	100	30.0
II	1	8	0.2	410	66	45.5
II	1	9	0.2	410	50	60.0
II	2	10	0.2	820	400	7.5
II	2	11	0.2	820	300	10.0
II	2	12	0.2	820	200	15.0
II	2	13	0.2	820	180	16.7
II	2	14	0.2	820	150	20.0
II	2	15	0.2	820	130	23.1
II	2	16	0.2	820	100	30.0
II	2	17	0.2	820	66	45.5
II	2	18	0.2	820	50	60.0
II	3	19	0.5	410	250	12.0
II	3	20	0.5	410	200	15.0
II	3	21	0.5	410	150	20.0
II	3	22	0.5	410	100	30.0
II	3	23	0.5	410	50	60.0

a) Configuration 1 *b*) Configuration 2 *c*) Configuration 3

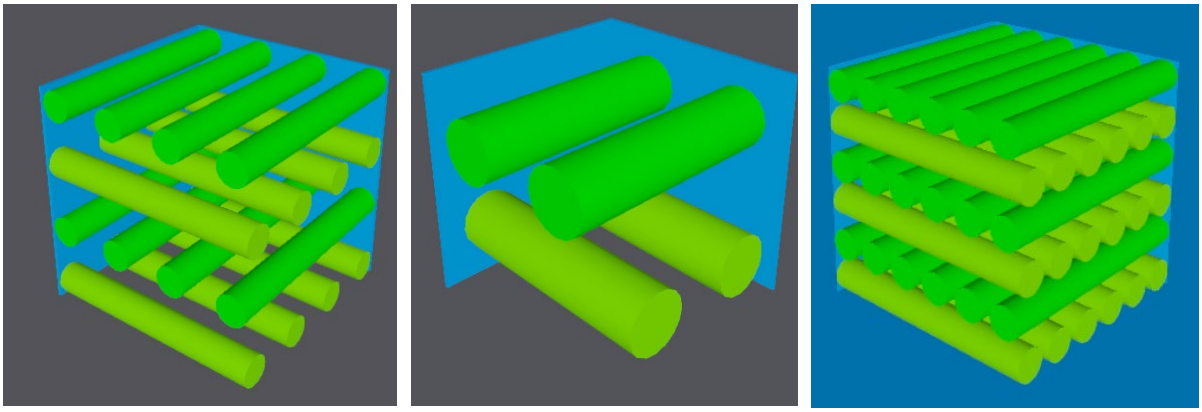

Figure 9. Geometry of modelled configurations within Campaign II.

3.3.2 Monitor points

Several monitor points were introduced at all positions where gauges were installed during the experiments. This report shows results only for two monitor points, WEST_4 and WEST_8, as depicted in Figure 10. These two monitor points are placed on the west wall at 1.87 m and 2.8 m from the ignition point, respectively.

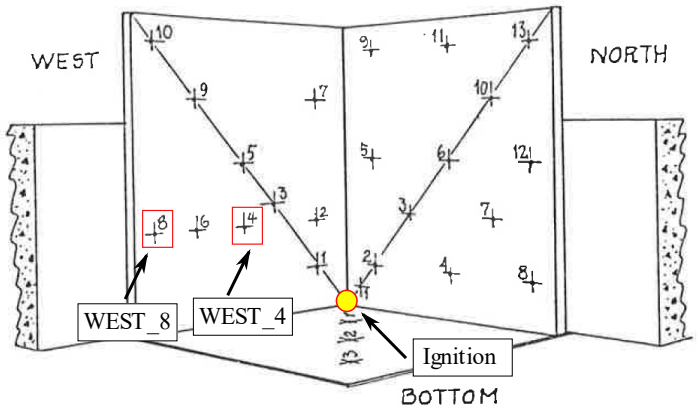

Figure 10. Location of relevant monitor points and ignition, Campaign II.

3.3.3 Initial turbulence conditions

The default initial conditions were used in this campaign, as defined below:

- Characteristic velocity: 200 m/s
- Relative turbulence intensity: 0.3
- Turbulence length scale: 0.05 m

3.3.4 Ignition

The ignition point was nominally placed at the innermost corner of the vessel, which represents the centre of the hemispherical explosion. The final position of the ignition point has though been adjusted to the closest cell centre for the different grid cell sizes. Care has been taken to ensure that the ignition points was placed on a completely unobstructed cell for all cases.

3.4 Stage I: Campaign III

3.4.1 Overview

In this campaign simulations of explosions of gas clouds surrounding a simplified vehicle are carried out. Only explosions of propane/air gas clouds with a stochiometric ratio were studied. In the different scenarios analysed, the dimensions of the gas cloud in the horizontal plane were kept constant, but the height, H, was varied. The main purpose of the campaign was to evaluate the current recommendations for choice of grid size based on the dimensions of the cloud. The general guidelines provided by (Gexcon AS, 2022) indicate that the grid size is chosen as a function of the smallest dimension of the cloud, whereby the number of cells along the smallest dimension should be at least 15. For all scenarios, the height of the cloud constituted the smallest dimension of the cloud. This means that the cell size would depend on the cloud height according to the grid guidelines.

Several grid sizes were studied. The cell size was chosen so that the number of cells lies in a range of 15 to 120 along the smallest dimension of the cloud. Thereafter, a number of grid cell sizes outside this range were chosen with the purpose of having identical grid sizes across all four scenarios. A summary of the chosen grid sizes is presented in Table 4. Observe that almost all chosen cell sizes are divisors of 0.5 m, and care has been taken to align the geometry to the grid lines.

Table 4. Summary of studied scenarios and corresponding cell sizes within Campaign III.

Campaign	Configuration	Scenario	Cloud height [mm]	Cell size, h [mm]	No. cells along cloud height, N
III	1	1	500	125.0	4
III	1	2	500	83.3	6
III	1	3	500	71.4	7
III	1	4	500	62.5	8
III	1	5	500	50.0	10
III	1	6	500	33.3	15
III	1	7	500	25.0	20
III	2	8	1000	125.0	8
III	2	9	1000	83.3	12
III	2	10	1000	71.4	14
III	2	11	1000	66.7	15
III	2	12	1000	62.5	16
III	2	13	1000	50.0	20
III	2	14	1000	25.0	40
III	3	15	1500	125.0	12
III	3	16	1500	83.3	18
III	3	17	1500	75.0	20
III	3	18	1500	71.4	21
III	3	19	1500	50.0	30
III	3	20	1500	25.0	60
III	4	21	3000	200.0	15
III	4	22	3000	150.0	20
III	4	23	3000	125.0	24
III	4	24	3000	83.3	36
III	4	25	3000	50.0	60

3.4.2 Geometry

The mock-up vehicle was modelled with a simplified geometry as depicted in Figure 11. The distance between the vehicle and the ground was assumed to be equal to 0.5 m. The body of the vehicle was modelled as a rectangular prism with dimension 5.0×2.0×1.0 m. The wheels were modelled as rectangular prisms with dimensions 1.0×0.5×0.5 m.

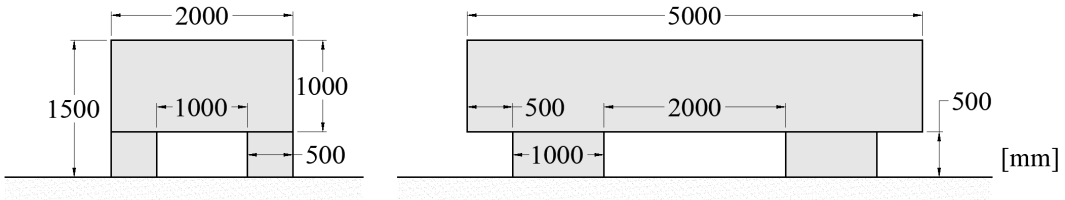

Figure 11: Geometry of mock-up vehicle within campaign III.

3.4.3 Equivalent gas cloud

A stochiometric premixed cloud of propane and air (equivalence ratio of 1.05) was assumed in all simulations. In the horizontal plane, the dimensions of the equivalent clouds are 6.0×3.0 m (length × width). Four different heights, H, were evaluated in this study:

- Configuration 1: H = 0.5 m
- Configuration 2: H = 1.0 m
- Configuration 3: H = 1.5 m
- Configuration 3: H = 3.0 m

An example of the modelled cloud is given in Figure 12 for two configurations.

a) Configuration 1, $H = 0.5$ m

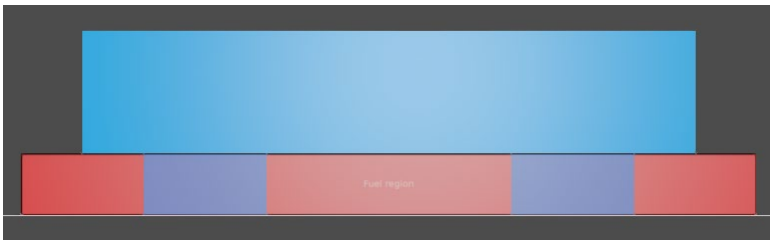

b) Configuration 2, $H = 1.0$ m

Figure 12: Equivalent gas cloud for configuration 1 and 2, within Campaign III.

3.4.4 Monitor points

A total of 14 monitor points were created to collect results from the simulations. Of particular interest in this study is monitor point BOT_14. This monitor point is placed at 3.0 m from the ignition point in the direction parallel to the vehicle. From the short edge of the vehicle, the monitor point is located at approximately 0.5 m. The monitor points are placed at an elevation of 0.2 m above the ground. The position of all monitor points is shown in Figure 13.

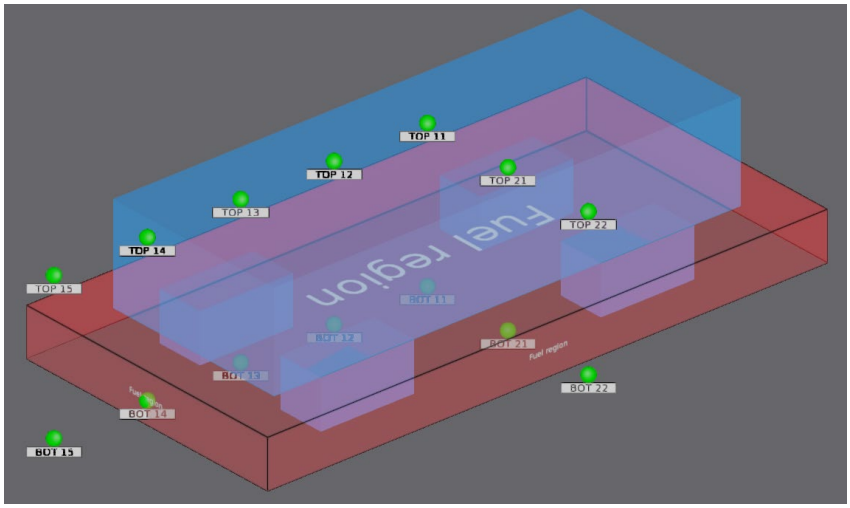

Figure 13: Monitor points in relation to the vehicle in Campaign III.

3.4.5 Initial conditions

The default initial conditions were used. No sensitivity analysis of these parameters was performed.

- Characteristic velocity: 200 m/s
- Relative turbulence intensity: 0.3
- Turbulence length scale: 0.05 m

3.4.6 Ignition

Ignition is assumed to take place in the centre of the confined region between the vehicle and the ground at an elevation of around 0.20 m. The final position of the ignition point has though been adjusted to the closest cell centre for the different grid cell sizes.

3.5 Stage I: Campaign IV

3.5.1 Overview

The aim of this campaign was to investigate the grid dependency in connection with the initial turbulence conditions. Explosions of equivalent propane/air gas clouds surrounding a mock-up vehicle were carried out. Three different initial turbulence conditions were considered. In this campaign, the grid cell size was defined as a function of the number of cells along the main direction of confinement. The confined region in the studied environment is the region under the vehicle. Therefore, the grid cell size is given by the number of cells along the distance between the underside of the vehicle and the ground, N_{veh}. A summary of the studied scenarios is given in Table 5.

A stochiometric premixed cloud of propane and air (equivalence ratio of 1.05) is assumed in all simulations. The shape of the equivalent cloud was set to 6.8×3.8×1.8 m (length × width × height).

Table 5. Summary of studied scenarios and corresponding cell sizes within Campaign IV.

Campaign	Configuration	Scenario	U [m/S]	TLS [m]	Cell size, h [mm]	No. cells along cloud height, N	No. cells under veh., N_{veh}
IV	1	1	60	0.05	100	18	3
IV	1	2	60	0.038	75	24	4
IV	1	3	60	0.025	50	36	6
IV	1	4	60	0.019	37.5	48	8
IV	1	5	60	0.0125	25	72	12
IV	2	6	1	0.05	100	18	3
IV	2	7	1	0.038	75	24	4
IV	2	8	1	0.025	50.0	36	6
IV	2	9	1	0.019	37.5	48	8
IV	2	10	1	0.0125	25	72	12
IV	3	11	0.1	0.05	100	18	3
IV	3	12	0.1	0.038	75	24	4
IV	3	13	0.1	0.025	50	36	6
IV	3	14	0.1	0.019	37.5	48	8
IV	3	15	0.1	0.0125	25	72	12

3.5.2 Geometry

The mock-up vehicle was modelled with a simplified geometry as depicted in Figure 14. The body of the vehicle was modelled as a rectangular prism with dimension 4.8×1.8×1.2 m. The wheels were modelled as rectangular prisms with dimensions 0.5×0.2×0.3 m. Observe that all dimensions are multiple of 50 mm and 20 mm, to facilitate alignment of the geometry and the grid.

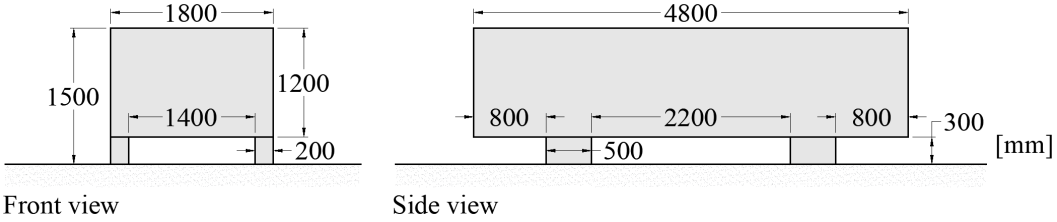

Figure 14. Geometry of mock-up vehicle within Campaign IV.

3.5.3 Monitor points

Several monitor points were created to collect results from the simulation. Of particular interest in this study is MP_9_9. This monitor point is placed at 3.0 m from the ignition point in the direction perpendicular to the vehicle (2.1 m from the long edge of the vehicle), see Figure 15. The monitor point is placed at an elevation of 0.2 m above the ground.

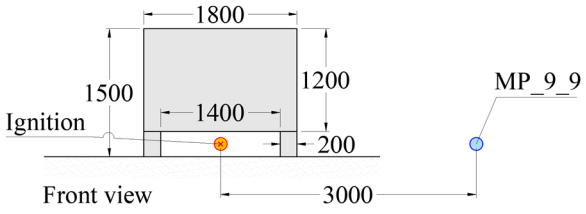

Figure 15. Location of relevant monitor point within Campaign IV.

3.5.4 Initial conditions

Three different values of the fluctuating velocity ($u' = U \cdot RTI$) were studied: 60, 1, and 0.1 m/s. Note that $u' = 60$ m/s corresponds to the default value. To choose the other two values, it was assumed that a relative turbulent intensity (RTI) of 10 %, representing relatively high turbulent conditions, was a reasonable upper limit for this parameter in this type of environment. Additionally, the initial characteristic velocity (U), dictated largely by the wind conditions, was assumed to lie between the values 1 m/s and 10 m/s.

The turbulent length scale (TLS) was chosen as a function of the smallest grid size as described below:

- Cell size ≥ 100 mm: $TLS = 0.05$ m (default value)
- Cell size < 100 mm: $TLS = 0.5 \times$cell size

3.5.5 Ignition

The ignition point was nominally placed in the space between the vehicle and the ground at the centre of the confined region and at an elevation of 0.2m. The final position of the ignition point has though been adjusted to the closest cell centre. Care has been taken to ensure that the ignition points is placed on a completely unobstructed cell for all cases.

3.6 Stage II: Campaign V

3.6.1 Overview

This campaign aims at identifying a suitable cell size for explosion simulations in which the flow is largely two-dimensional. To achieve the intended objective, an experimental study available in the literature was simulated with the CFD code with different grid cell sizes. The chosen experiment consists of a study of the deflagration of an ethylene-air mixture in a congested region confined between two planes in which obstruction was introduced with parallel horizontal tubes (van Wingerden, 1984). Besides the effects of the obstacles on flame propagation, the influence of the distance between planes and the porosity of the top plate was evaluated in this study. Available results include values of flame speed inside the confined region and peak overpressure outside the confined region. This experiment was chosen as the basis for the choice of grid cell size, as results for both flame velocity and overpressure both inside and outside the confined region are available. The general set-up of the experiment appears in Figure 16.

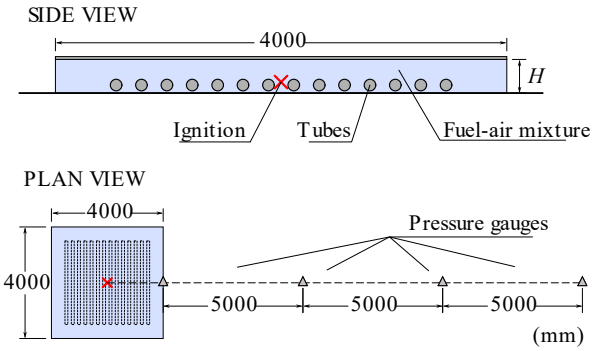

Figure 16. Set-up of experiment simulated in Campaign V, adapted from (van Wingerden, 1984).

Three values of the height of the top plate, H, were considered here: 0.12, 0.30 and 1.0 m. The largest ratio between the length of the confining plates and the distance between plates (L/H) for the studied configurations was 4, which is the usually accepted limit for a case dominated by two-dimensional confinement (Center for Chemical Process Safety, 2010). A summary of the scenarios carried out as part of this campaign are given in Table 6. Here, the grid cell size is given by the number of cells along the distance between plates, N_H. The geometry of the configuration as modelled in FLACS are shown in Figure 17.

Table 6. Summary of studied scenarios and corresponding cell sizes within Campaign V.

Campaign	Configuration	Scenario	H [m]	U [m/S]	TLS [m]	Cell size, h [mm]	No. cells along dir. confinement, N_H
V	1.1	1	0.3	1	0.03	100.0	3
V	1.1	2	0.3	1	0.025	50.0	6
V	1.1	3	0.3	1	0.021	42.9	7
V	1.1	4	0.3	1	0.019	37.5	8
V	1.1	5	0.3	1	0.015	30.0	10
V	1.1	6	0.3	1	0.01	20.0	15
V	1.2	7	0.3	0.1	0.03	100.0	3
V	1.2	8	0.3	0.1	0.025	50.0	6
V	1.2	9	0.3	0.1	0.021	42.9	7
V	1.2	10	0.3	0.1	0.019	37.5	8
V	1.2	11	0.3	0.1	0.015	30.0	10
V	1.2	12	0.3	0.1	0.01	20.0	15
V	1.3	13	0.3	60	0.03	100.0	3
V	1.3	14	0.3	60	0.025	50.0	6
V	1.3	15	0.3	60	0.019	37.5	8
V	1.3	16	0.3	60	0.015	30.0	10
V	2	17	1.0	1	0.05	333.3	3
V	2	18	1.0	1	0.05	166.7	6
V	2	19	1.0	1	0.05	125.0	8
V	2	20	1.0	1	0.05	100.0	10
V	3	21	0.12	1	0.012	40.0	3
V	3	22	0.12	1	0.01	20.0	6
V	3	23	0.12	1	0.008	15.0	8

a) Configuration 1 ($H = 0.3$ m, $L/H = 13.3$)

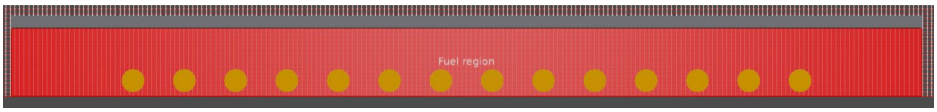

b) Configuration 2 ($H = 1.0$ m, $L/H = 4.0$)

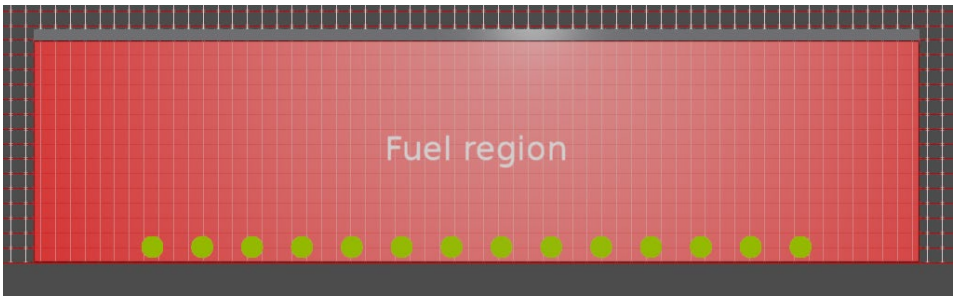

c) Configuration 3 ($H = 0.12$ m, $L/H = 33.3$)

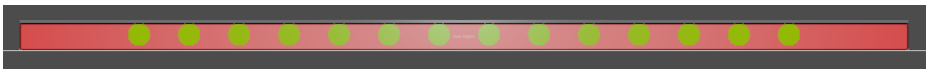

Figure 17. Set-up of the different configurations in Campaign V, as modelled in FLACS-CFD.

3.6.2 Equivalent gas cloud

A stochiometric premixed cloud of ethylene and air (equivalence ratio of 1.13) was assumed in the simulations. The cloud was assumed to fill the entire space between confining plates.

3.6.3 Result line and monitor points.

The results were extracted from the cells located along a path crossing the centre of the configuration. The path lies perpendicularly to the obstructing tubes. Several monitor points were created to collect results from the simulation, both inside and outside the configurations. Of particular interest in this report is monitor point MP_10_6, which is located at 3.0 m from the ignition centre (1.0 m outside the configuration). Figure 18 shows the location of the result line and the chosen monitor point.

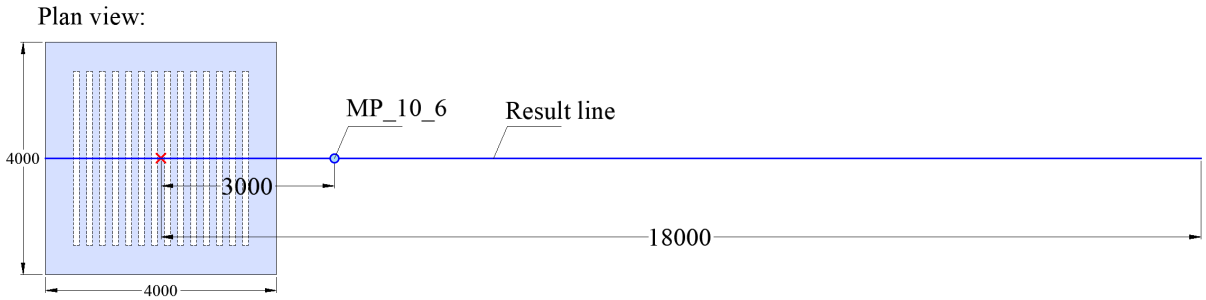

Figure 18. Location of relevant monitor point and result line in Campaign V.

3.6.4 Initial turbulence conditions

The reference value of the fluctuating velocity ($u' = U \cdot RTI$) for the simulations was 1 m/s. This value was used for all the configurations. Furthermore, two other values of the fluctuating velocity were studied for configuration 1 to investigate the sensitivity of the results to this parameter. These two additional values were 60 m/s (default value) and 0.1 m/s.

The turbulent length scale (*TLS*) was chosen as a function of the smallest grid as described below:

- Cell size ≥ 100 mm: *TLS* = 0.05 m (default value)
- Cell size < 100 mm: *TLS* = 0.5×cell size

3.6.5 Ignition

The ignition point was nominally placed the centre of the configuration at an elevation of 0.15 m for configurations 1 and 2 and at an elevation of 0.06 m for configuration 3. The final position of the ignition point was adjusted to the closest cell centre. Care has been taken to ensure that the ignition points is placed on a completely unobstructed cell for all cases.

3.6.6 Experimental results

The maximum overpressure measured in the experiments reported in (van Wingerden, 1984) are presented in Figure 19. The relevant results for the modelled configurations are highlighted with coloured circles. The measured flame speed for configuration 1 (*H* = 0.3 m) is given in Figure 20.

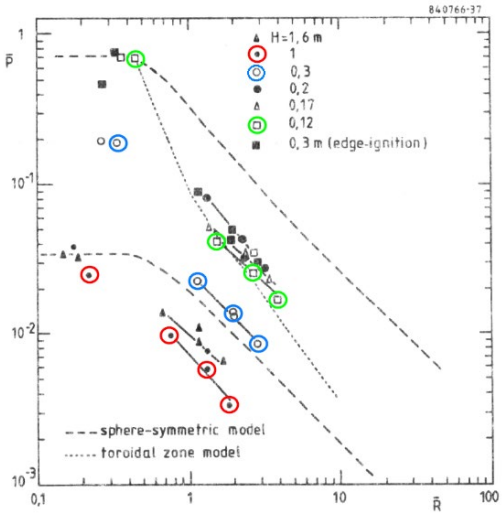

Fig. 37 Decay of blast due to explosions within a double plate configuration with obstacles (P = 2,25 D; h = 0,2 D; 7-8% v/v ethylene-air; large-scale tests)

Distance [m]	*H* [m]		
	0.12	**0.3**	**1.0**
2	70.0	19.00	2.45
7	4.2	2.30	1.00
12	2.5	1.40	0.60
17	1.7	0.85	0.34

Figure 19: Measured values of overpressure for different heights of the top plate in (van Wingerden, 1984). Modified to highlight relevant results for H = 1.0 m (red), H = 0.3 m (blue) and H = 0.12 m (green).

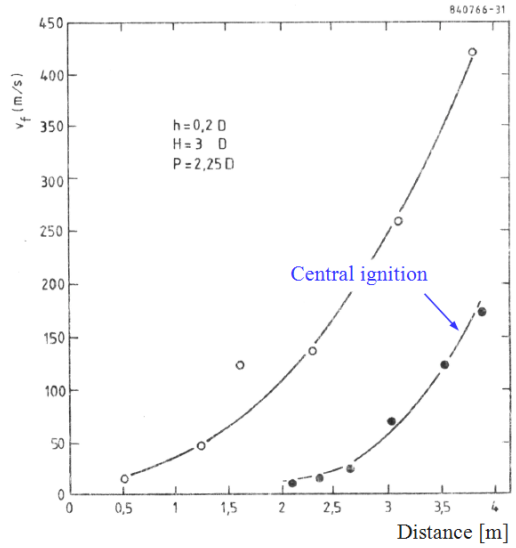

Figure 20: Flame speed as a function of distance of a centrally ignited and edge-ignited explosion in the double plate configuration with H = 0.3 m (7/8 % ethylene-air) in (van Wingerden, 1984).

3.7 Stage II: Campaign VI

3.7.1 Overview

This campaign is part of the Stage II, which aims at identifying a suitable cell size for explosion simulations in a two-dimensional confinement. In this campaign, the conclusions from Campaign V regarding choice of grid cell size are implemented during modelling with the purpose of testing the performance.

Similarly to the experiment simulated in Campaign V, the experiment evaluated in Campaign VI (which is often referred to as DISCOE in the literature), also deals with deflagrations between two parallel planes. However, the configuration in the DISCOE experiment was provided with obstacles in the form of vertical tubes in a radial arrangement (van Wingerden, 1989). The effects of pitch, confinement, gas reactivity, and distance between congested regions were studied. From this experiment, values of flame speed inside the confined region are available for different gases, including ethylene and propane. The geometry of the experiment is presented in Figure 21. The dimension of the confining plates is 4×2 m. A wall of symmetry was installed at one of the long sides. The distance between parallel plates, *H*, was 0.16 m. The ratio *B*/*H* for this configuration is 12.5.

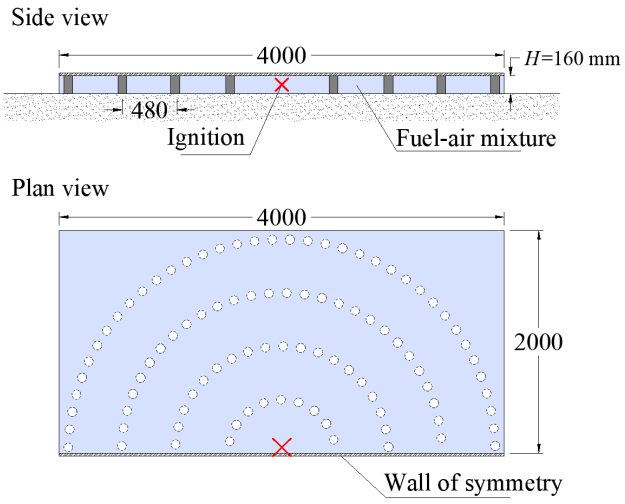

Figure 21. Set-up of experiment simulated in Campaign VI, adapted from (van Wingerden, 1989).

The scenarios analysed within this campaign are summarised in Table 7. Note that the gas used in configuration 1 (ethylene) is the same gas as the one used in Campaign V. However, propane was used in configuration 2.

Table 7. Summary of studied scenarios and corresponding cell sizes within Campaign VI.

Campaign	Configuration	Scenario	Gas	H [m]	U [m/S]	TLS [m]	Cell size, h [mm]	No. cells along dir. confinement, N_H
VI	1	1	Ethylene	0.16	1.0	0.0266	53.3	3
VI	1	2	Ethylene	0.16	0.1	0.0266	53.3	3
VI	1	3	Ethylene	0.16	1.0	0.0133	26.7	6
VI	1	4	Ethylene	0.16	0.1	0.0133	26.7	6
VI	2	5	Propane	0.16	1.0	0.0266	53.3	3
VI	2	6	Propane	0.16	0.1	0.0266	53.3	3
VI	2	7	Propane	0.16	1.0	0.0133	26.7	6
VI	2	8	Propane	0.16	0.1	0.0133	26.7	6

3.7.2 Equivalent gas cloud

For configuration 1, a stochiometric premixed cloud of ethylene and air (equivalence ratio of 1.13) was used. For configuration 2, a stochiometric premixed cloud of propane and air (equivalence ratio of 1.05) was assumed in the simulations. The cloud was assumed to fill the entire space between confining plates.

3.7.3 Monitor points

The results were extracted from monitor points located along several radial results path with the ignition point as starting point. The position of the result paths is given in Figure 22.

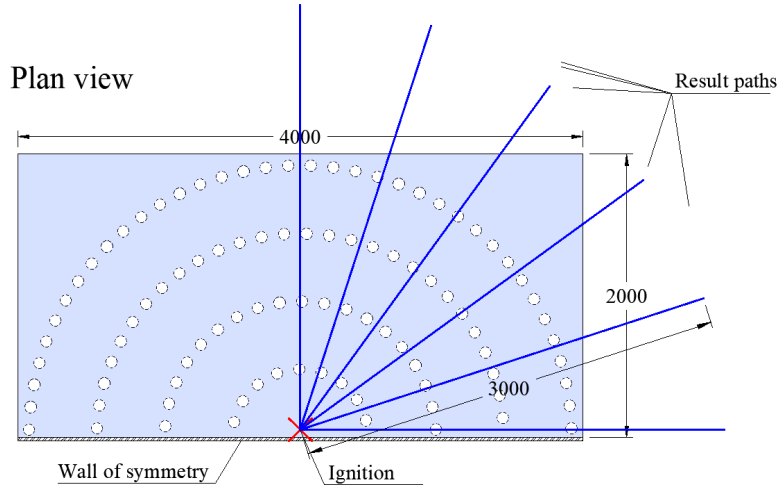

Figure 22. Location of result paths in Campaign VI.

3.7.4 Initial conditions

Two different values of the fluctuating velocity ($u' = U \cdot RTI$) were studied: 1, and 0.1 m/s. To calculate these values, the relative turbulent intensity (RTI) was set to 10 %. The initial characteristic velocity (U), given by the wind flow created by the fans, was assumed to lie between the extreme values 1 m/s and 10 m/s.

The turbulent length scale (TLS) was chosen as a function of the smallest grid size as described below:

- Cell size ≥ 100 mm: TLS = 0.05 m (default value)
- Cell size < 100 mm: TLS = 0.5×cell size

3.7.5 Ignition

The ignition point was nominally placed at the centre of the wall of symmetry at an elevation of 0.08 m. The final position of the ignition point was adjusted to the closest cell centre. Care has been taken to ensure that the ignition points is placed on a completely unobstructed cell for all cases.

3.7.6 Experimental results

Figure 23 gives the flame speed measured in the experiments reported in (van Wingerden, 1989) for the cases with a ethylene-air mixture. Only results for $P = 6D$ are relevant in this report. Here, P is the pitch (distance between obstacles), and D is the obstacle diameter.

Figure 24 gives the nondimensionalized flame speed for the three types of gases tested in the experiments. The laminar flame speed of each gas according to (Bradley, 1978) can be used to convert the results to flame speed in units of length/second.

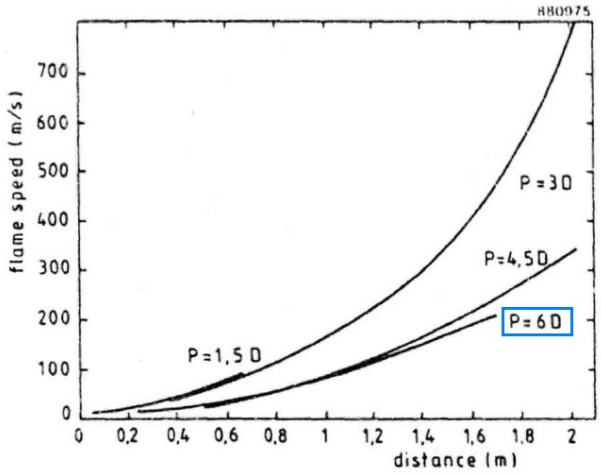

Figure 23. Flame speed development for various values of pitch P in the experiment in (van Wingerden, 1989). Test conditions: H =160 mm, gas = 7.5 % ethylene. The relevant results in this report are those for P = 6D.

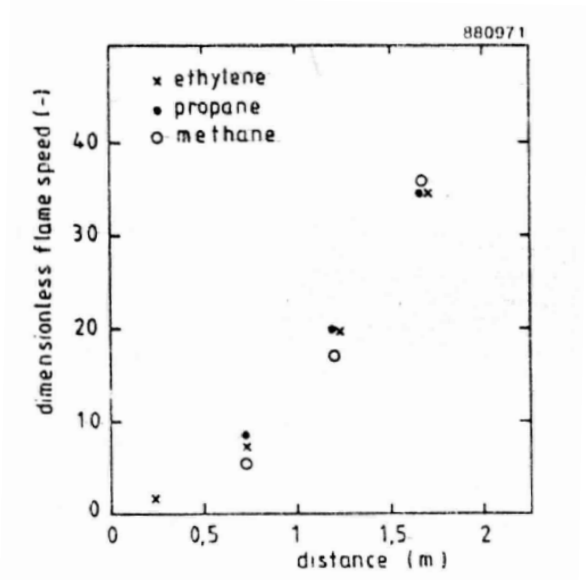

Figure 24. Nondimensional flame speed as a function of distance and gas type in the experiment in (van Wingerden, 1989). Test conditions: H =160 mm, gas = 7.5 % ethylene, pitch = 6D. The laminar flame speed of each gas must be used to calculate the flame speed in units of length/second.

4 Results

4.1 General

The results presented in this chapter are intended for evaluating the grid dependency on the resulting peak overpressure and peak impulse, as described in Section 2.2. The overpressure is the difference between the absolute pressure and the ambient pressure. The impulse is defined as the integral of the overpressure-time history. When the overpressure is in the positive phase, the impulse will increase as time progresses. Conversely, when the overpressure is in the negative phase, the impulse will decrease with time. The peak impulse is the maximum impulse during the simulation time.

For a given campaign, the results are only presented at a few selected monitor points. This to facilitate the analysis of the results for a large number of scenarios. However, the results at other monitor points in the region of interest were investigated to ensure that the conclusions reached in this report are in general applicable for the entire region of interest within a given scenario.

The results for each campaign are presented individually in their own section within this chapter. A general evaluation of the results as well as comparison between the different campaigns is carried out in Chapter 5.

4.2 Stage I: Campaign I

The results from this campaign were gathered from monitor points BOT_14 (located at 3.0 m from the ignition point in the direction parallel to the vehicle) and BOT_22 (located at 2.0 m from the ignition point in the direction perpendicular to the vehicle), see Figure 4. Figure 25a) gives the variation of the peak overpressure as a function of the number of cells along the smallest dimension of the cloud, N, at BOT_14. The same figure gives the results for the configuration with an unconfined and unobstructed cloud as well as for the configuration with a vehicle centrally placed inside the cloud. In Figure 25b) the same data is instead presented as a function of the grid cell size, h. A strong grid dependency can be discerned in the figures: refining the grid consistently leads to an increased overpressure. Moreover, the relationship between the peak overpressure and N appears to be nearly linear for the unconfined configuration. The results indicate that further refinement is likely to continue producing greater overpressure. The error in the prediction of peak overpressure at BOT_14 between consecutive grid resolutions ranges between 18 %[4] and 54 %[5].

The influence of the grid resolution on the peak impulse at BOT_14 is presented in Figure 26. Similarly to the observed trend for the peak overpressure, a clear grid dependency can be observed for the peak impulse, in that finer grids produce greater peak impulse. The error in the prediction of peak impulse between consecutive grid resolutions at BOT_14 ranges between 9 % and 28 %. That is, the effect of the grid size appears to be less pronounced, though still significant, for the peak impulse.

Similar conclusions can be made at monitor point BOT_22 based on the results shown in Figure 27 and Figure 28. The error in the prediction of peak overpressure between consecutive grid resolutions at BOT_22 ranges between 20 %[6] and 60 %[7], while the error in the prediction of peak impulse varies between 9 % and 28 %.

[4] Between scenario 5 (h = 80 mm) and scenario 6 (h = 50 mm)
[5] Between scenario 2 (h = 200 mm) and scenario 3 (h = 150 mm)
[6] Between scenario 5 (h = 80 mm) and scenario 6 (h = 50 mm)
[7] Between scenario 2 (h = 200 mm) and scenario 3 (h = 150 mm)

a) Peak overpressure vs No. cells

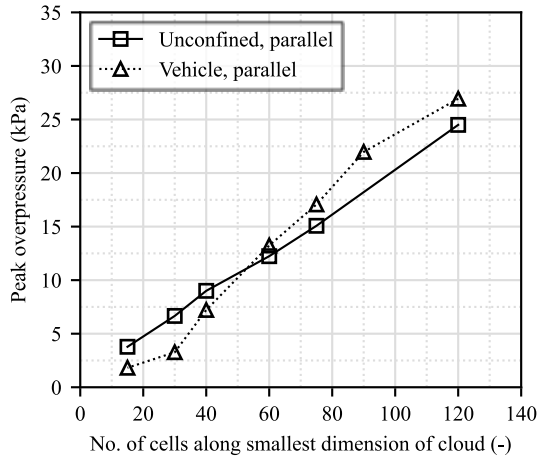

b) Peak overpressure vs cell size

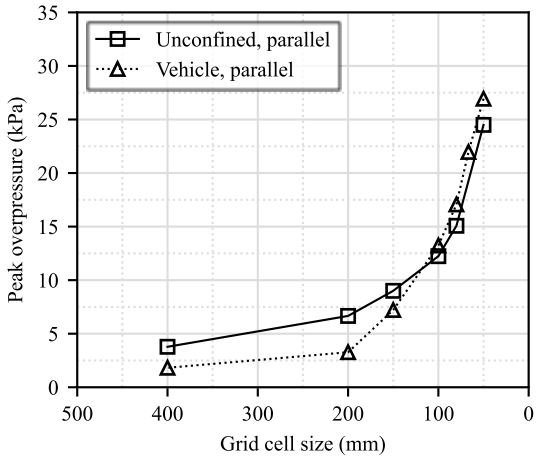

Figure 25. Peak overpressure at monitor point BOT_14 (at 3 m from the ignition point in the main direction of the vehicle) for different grid resolutions. Campaign I.

a) Peak impulse vs No. cells

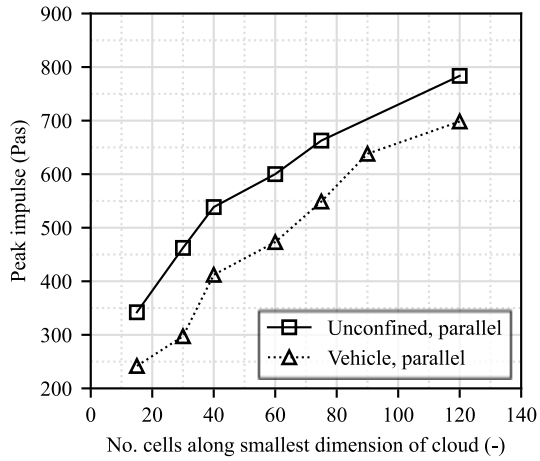

b) Peak impulse vs cell size

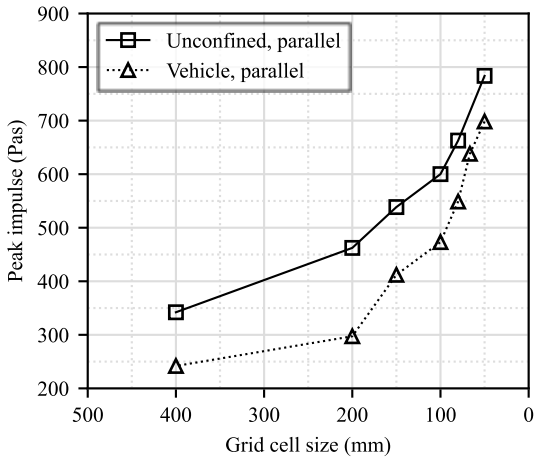

Figure 26. Peak impulse at monitor point BOT_14 (at 3 m from the ignition point in the main direction of the vehicle) for different grid resolutions. Campaign I.

a) Peak overpressure vs No. cells

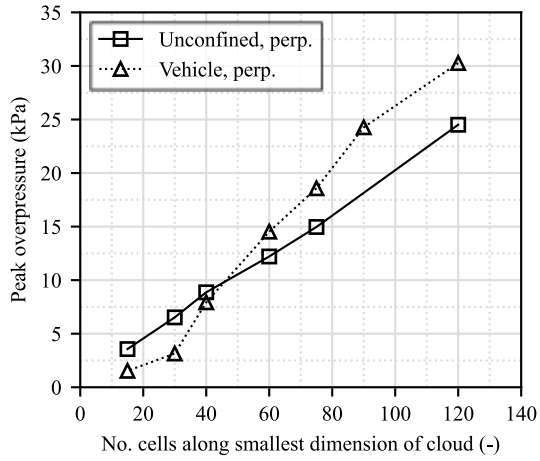

b) Peak overpressure vs cell size

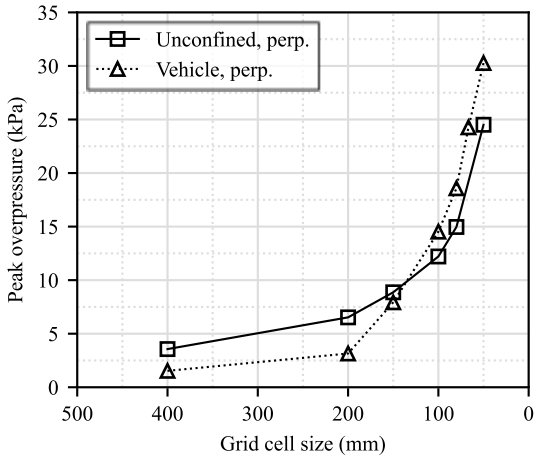

Figure 27. Peak overpressure at monitor point BOT_22 (at 2 m from the ignition point in the direction perpendicular to the main direction of the vehicle) for different grid resolutions. Campaign I.

a) Peak impulse vs No. cells

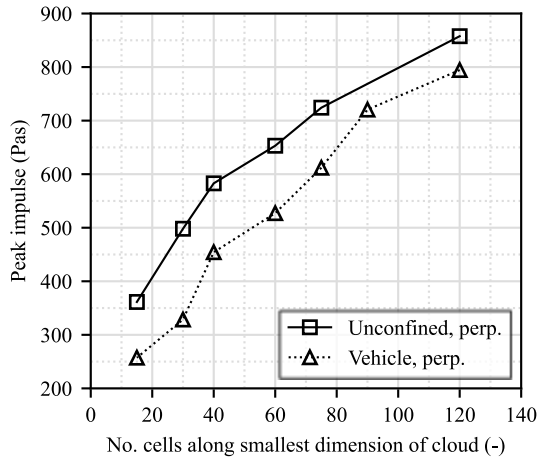

b) Peak impulse vs cell size

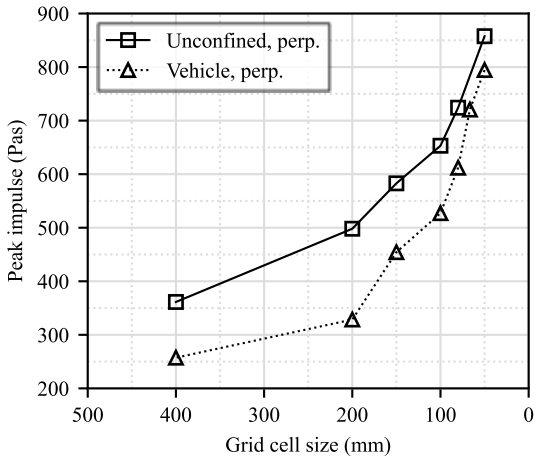

Figure 28. Peak impulse at monitor point BOT_22 (at 2 m from the ignition point in the direction perpendicular to the main direction of the vehicle) for different grid resolutions. Campaign I.

Two additional observations can be made regarding these results:

- The expected enhancing effect of the confinement under the vehicle, compared with a completely unconfined cloud, only becomes evident for scenarios with more than 50 or 60 cells along the height of the cloud. That is, those scenarios with a grid cell size equal to or less than around 100 or 120 mm.
- The peak overpressure values at BOT_14 and BOT_22 for the unconfined configuration are very similar for a given grid resolution, even though BOT_22 is located one meter closer to the ignition point. However, for the configuration with a vehicle, the results at these two monitor points differ at all grid resolutions. For scenarios with $N \leq 30$ ($h \geq 200$ mm), the peak overpressure is about 10 % smaller at BOT_22, while for $N > 30$, the peak overpressure at BOT_22 is in average 10 % greater at BOT_22. Based on the current state of the art, it is expected that the pressure at BOT_22 be greater due to the closer distance to ignition centre.

The fact that it is not so for the coarser grids indicate that, for those scenarios, the solution is not physically reasonable.

The likely common denominator for the two observations presented above is the combustion that occurs in the confined zone under the vehicle. To capture these two important aspects, it appears that the grid cell size should be in the order of 100 to 120 mm, or less. This could be translated to at least 3 to 4 cells in the confined region under the vehicle to properly resolve the combustion process in this region.

4.3 Stage I: Campaign II

The results are presented for the monitor points WEST_4 and WEST_8, which are located on the west wall at 1.87 m and 2.8 m from the ignition point, see Figure 10. Figure 29 shows the relationship between the peak overpressure and *a*) the number of cells along the side of the cloud and *b*) the grid cell size for configuration 1.

a) Peak overpressure vs No. cells

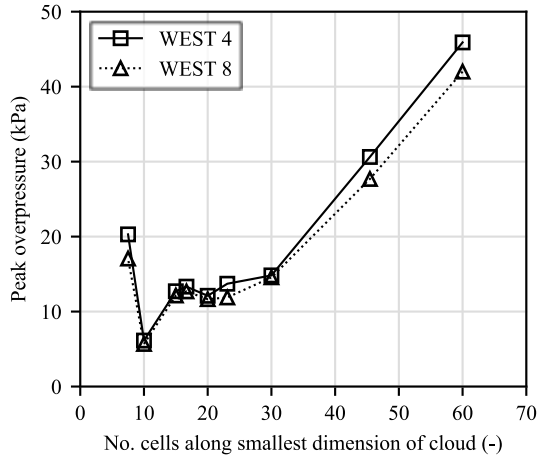

b) Peak overpressure vs grid cell size

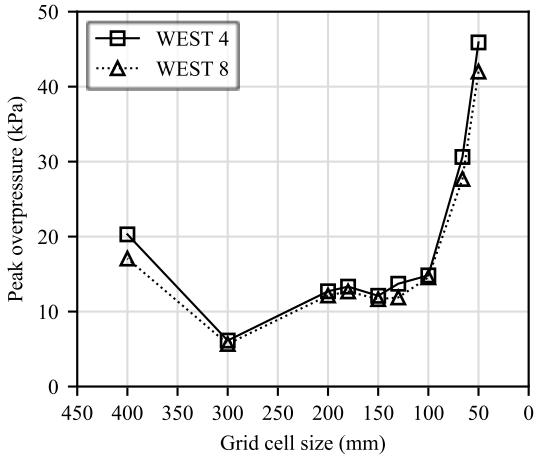

Figure 29. Peak overpressure at selected monitor points for configuration 1 (VBR = 0.2, D = 410 mm) within Campaign II.

Three different zones can be discerned along these curves:

- Zone 1: For scenarios with $N \leq 10$, the solution appears to oscillate with a large amplitude, which may indicate that the flow cannot be resolved correctly with so few cells in the cloud. However, it should be noted that a user should not use this low number of cells, as the grid guidelines require at least 15 cells along the side of the cloud.
- Zone 2: For scenarios with $15 \leq N \leq 30$, the solution appears to have achieved an oscillatory convergence (with small amplitude) around approximately 13 kPa. In fact, the solution in zone 1 could possibly be claimed to oscillate around this value as well. For the normal user, these results would be satisfactory, and further refinement would probably not have been carried out. The greatest overpressure measured in the experiments was in the order of 2 kPa (B. Hjertager et al., 1988), which means that the converged value of 13 kPa is greater than the experimental value. Thus, an experienced user may judge the converged value reasonable and conservative and may conclude that it is not necessary to continue refining the grid.
- Zone 3: Further refinement of the mesh causes a sudden significant increase in overpressure. This may indicate that, for this particular scenario, the sub-grid model for explosion breaks down for $N > 30$.

The error in the prediction of peak overpressure between consecutive grid resolutions for configuration 1 ranges between 5 % and 52 % for WEST_4 and between 4 % and 47 % for WEST_8, excluding the results in zone 1.

In Figure 30 the peak impulse is plotted against *a*) the number of cells along the smallest cloud dimension and *b*) the grid cell size for configuration 1. Here, the increase of peak impulse after a short interval of local convergence occurs sooner, at $N > 20$ (grid cell size < 150 mm). Thus, even though convergence could be motivated up to $N = 30$ for peak overpressure, the duration of the positive phase increases markedly already for $N \geq 20$. However, the error in the prediction between consecutive grid resolutions is in general lower for the peak impulse. This error ranges between 1 % and 23 % for WEST_4 and between 1 % and 24 % for WEST_8, excluding the results in zone 1.

a) Peak impulse vs No. cells

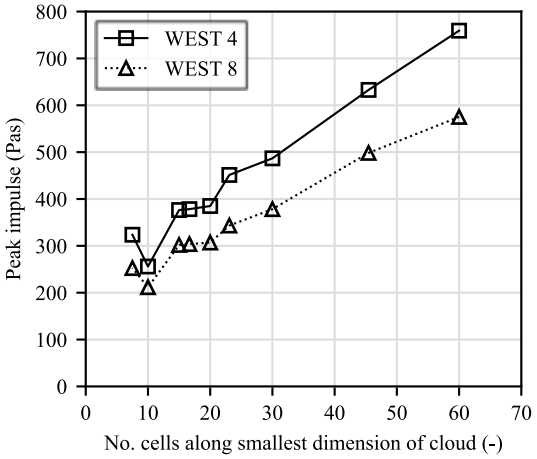

b) Peak impulse vs grid cell size

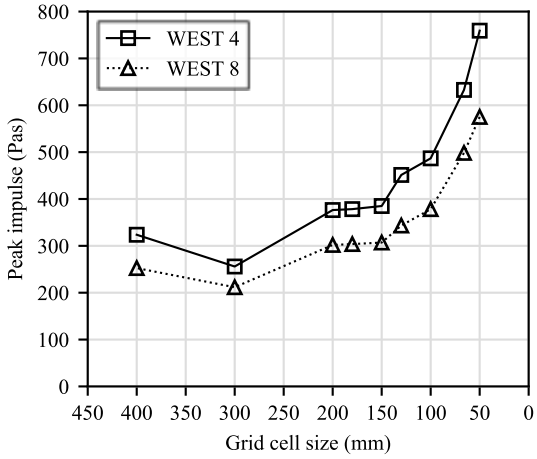

Figure 30. Peak impulse at selected monitor points for configuration 1 (VBR = 0.2, D = 410 mm) within Campaign II.

Similar results can be observed for configuration 2 in Figure 31 and Figure 32. That is, the solution appears to reach oscillatory convergence of the peak overpressure for $15 \leq N \leq 30$. Moreover, oscillatory convergence may be claimed for the peak impulse for $15 \leq N \leq 20$. However, both parameters increase rapidly after further refinement. The maximum overpressure experimentally measured for this configuration is in the order of 25 kPa (B. Hjertager et al., 1988), while the numerical results show around 35 kPa in the locally converged interval. The similar trend in the results from configurations 1 and 2 is probably connected to the diameter of the obstacles, which is the same in both configurations ($D = 410$ mm).

a) Peak overpressure vs No. cells

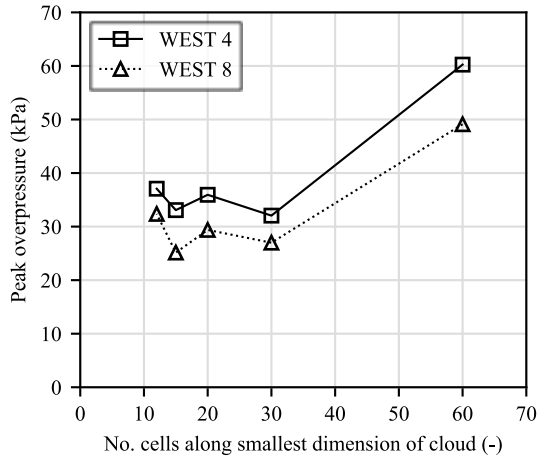

b) Peak overpressure vs grid cell size

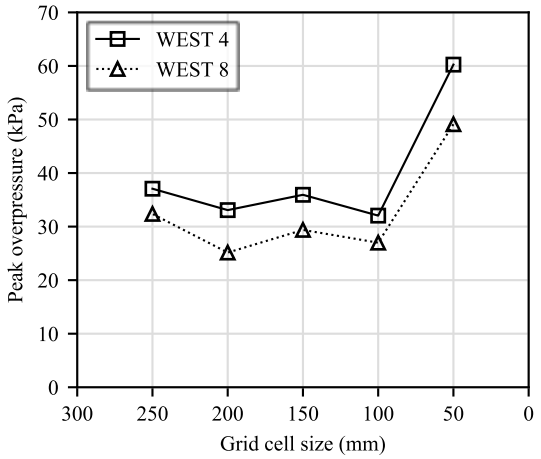

Figure 31. Peak overpressure at selected monitor points for configuration 2 (VBR = 0.5, D = 410 mm) within Campaign II.

a) Peak impulse vs No. cells

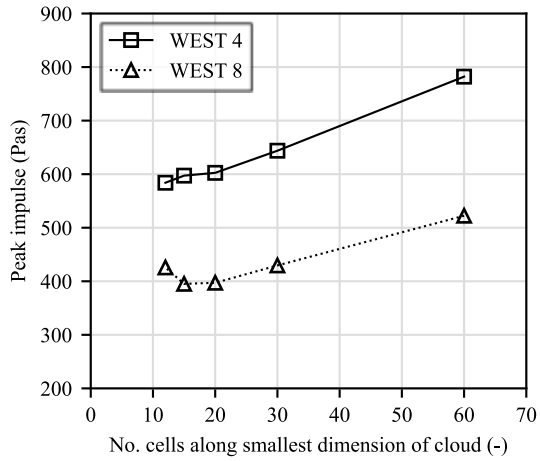

b) Peak impulse vs grid cell size

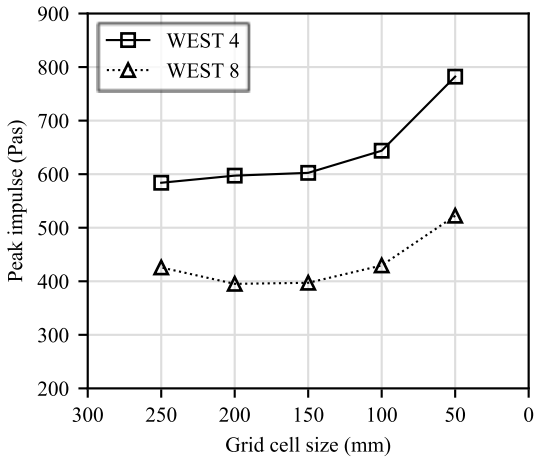

Figure 32. Peak impulse at selected monitor points for configuration 2 (VBR = 0.5, D = 410 mm) within Campaign II.

Configuration 3, in which $D = 820$ mm, shows no sign of convergence, as observed in Figure 33 and Figure 34. This may indicate that the code is better suited for configurations with small and repetitive obstacles but may struggle with scenarios with larger obstacles. The maximum overpressure measured for this configuration was in the order of 2 kPa (B. Hjertager et al., 1988), which is relatively similar to the results obtained with $10 \leq N \leq 20$.

It is worth noting that using $15 \leq N \leq 30$ would have given "acceptable" results for all three configurations, even if convergence was not clear. Here, "acceptable" means that the order of magnitude of the overpressure was captured by the software, although overprediction was obtained for all cases. Hence, for this type of configuration (highly congested with tube-like repetitive obstacles), following the guidelines would provide adequate results. The overpressure was overestimated in all configurations, but that could potentially be related to the effect of the initial turbulence conditions, which by default was assumed to be very high (although the effects of the initial turbulence are expected to be less important for highly dense configurations).

a) Peak overpressure vs No. cells

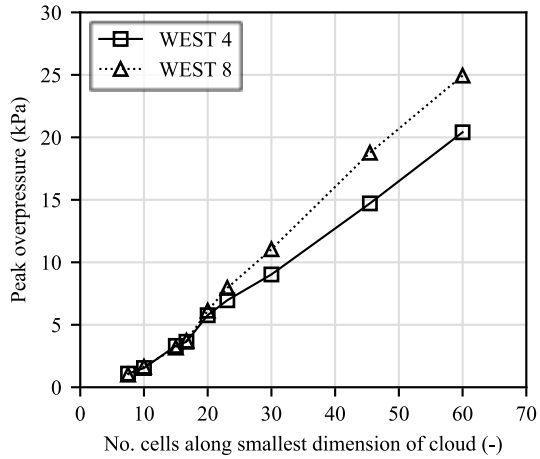

b) Peak overpressure vs grid cell size

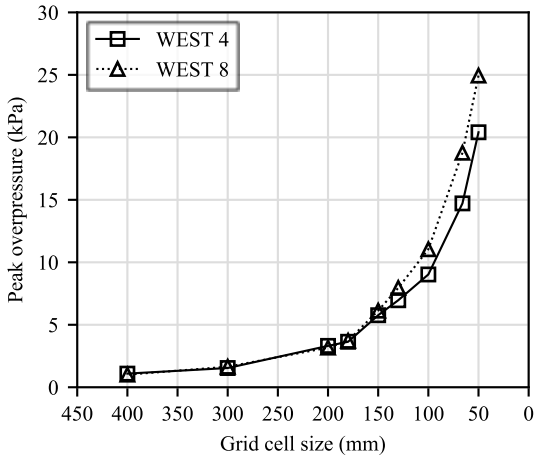

Figure 33. Peak overpressure at selected monitor points for configuration 3 (VBR = 0.2, D = 820 mm) within Campaign II.

a) Peak impulse vs No. cells

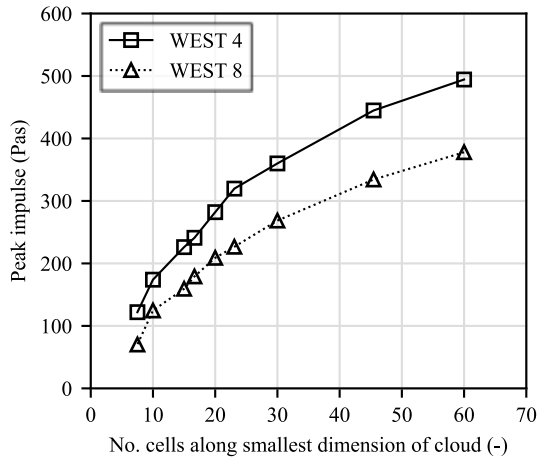

b) Peak impulse vs grid cell size

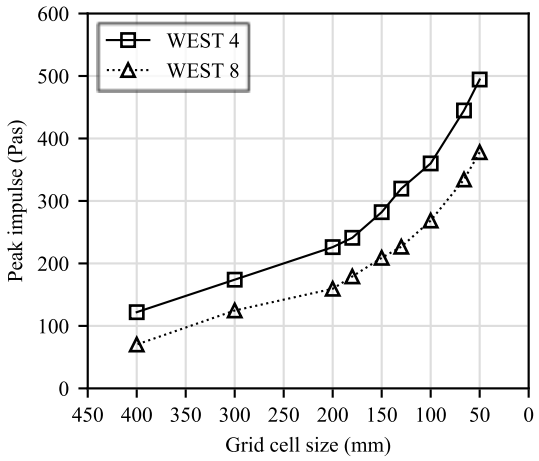

Figure 34. Peak impulse at selected monitor points for configuration 3 (VBR = 0.2, D = 820 mm) within Campaign II.

4.4 Stage I: Campaign III

The results are gathered from a monitor point located at three meters from the ignition point (0.5 m from the short edge of the vehicle), see Figure 13. Figure 35 gives the relationship between the peak overpressure and the number of cells along the smallest dimension of the cloud, *N*. A clear grid dependency can be discerned for all configurations.

Figure 35a) gives the relationship between the peak overpressure and the number of cells along the height of the cloud. For a given value of *N*, it can be observed that the calculated value of peak overpressure is greater for clouds with smaller height, *H*. That is, if the discretization of the cloud is done in accordance with the guidelines (based on the number of cells as a function of the smallest cloud dimension), the scenario with the smallest gas volume ($H = 0.5$ m) would produce the greatest overpressure. However, according to current state of art, it is expected that the smallest clouds produce lower overpressure, or at least similar results.

The same results are presented as plots of peak overpressure as a function of the grid cell size in Figure 35b). For the data arranged in this manner, it can be observed that very similar results are obtained for cases with different cloud height but same grid size. This time, the configuration with $H = 0.5$ m shows the lowest pressure values for a given cell size, while configurations with $H \geq 1.0$ m show similar results, although a subtle trend for higher pressure for greater H can be discerned. These results are more physically correct. This implies that for this type of scenarios, it is more correct to define the grid cell size in absolute values, rather than define it as a function of the cloud dimension.

a) Peak overpressure vs No. cells

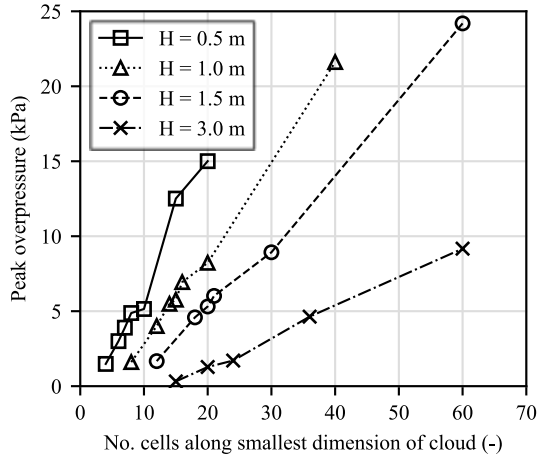

b) Peak overpressure vs grid cell size

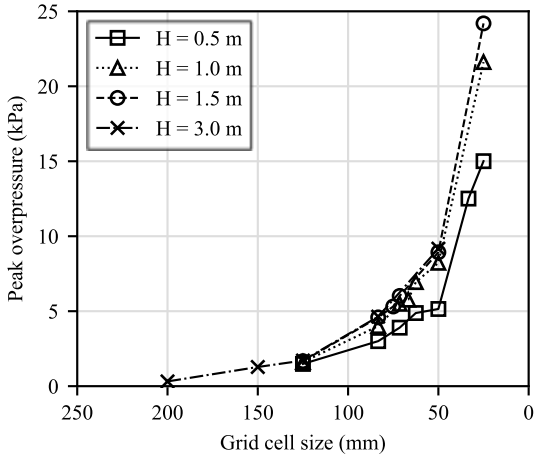

Figure 35. Peak overpressure at monitor point BOT_14 within Campaign III.

Table 8 gives the minimum and maximum error in the prediction between two consecutive grid resolutions. It should be noticed that the minimum error is not obtained for the finest grid, but instead occurs in the middle of the range of grid resolutions tested, where some grid cell sizes are similar (e.g., 71, 75, 83 mm). Likewise, the maximum error does not necessarily occur for the coarsest cell sizes. In fact, for some cases the maximum error was obtained between the two finest cell sizes.

Table 8. Maximum and minimum error in the prediction of peak overpressure (e_p) and peak impulse (e_i) between two consecutive grid resolutions.

Cloud height, H [m]	$e_{p.min}$ **[%]**	$e_{p.max}$ **[%]**	$e_{i.min}$ **[%]**	$e_{i.max}$ **[%]**
0.5	5	59	10	39
1.0	5	62	2	32
1.5	12	64	0	32
3.0	25	75	7	22

Similar conclusions could be drawn for the peak impulse, based on the results shown in Figure 36. First, a strong grid dependency is evident for the peak impulse. Moreover, defining the grid cell size as a fraction of the cloud dimension may lead to inaccurate and physically incorrect results. Lastly, it appears that it is more appropriate to use absolute values of grid cell size.

a) Peak impulse vs No. cells

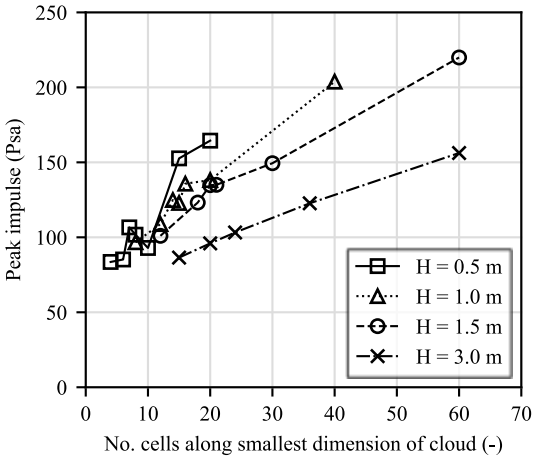

b) Peak impulse vs grid cell size

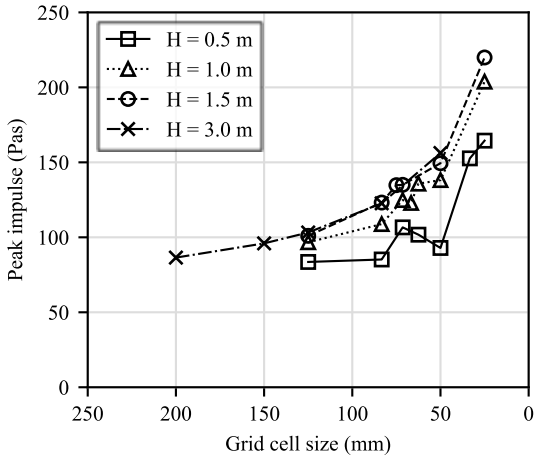

Figure 36. Peak impulse at monitor point BOT_14 within Campaign III.

Even though basing the cell size on the geometry of the cloud does not appear to work properly for this type of environment, it may still be reasonable to define the cell size based on the dimension of the confined region in the main direction of confinement. In this case, this corresponds to the distance between the vehicle and ground. Figure 37a) shows the peak overpressure as function of the number of cells under the vehicle, N_{veh}, while Figure 37b) shows the peak impulse as function of N_{veh}. For the data arranged in this manner, it can be seen that scenarios with $H \geq 1.0$ m give similar results, while the scenarios with $H = 0.5$ m produce the lowest values of peak overpressure and peak impulse. It should be noted that the distance between the ground and the underside of the vehicle is 0.5 m for all configurations. The results show that the clouds with a height greater than the height of the confined region under the vehicle produce similar results, while the clouds with height equal to or less than the height of the confined region produce lower overpressure.

a) Peak overpressure vs No. cells under vehicle

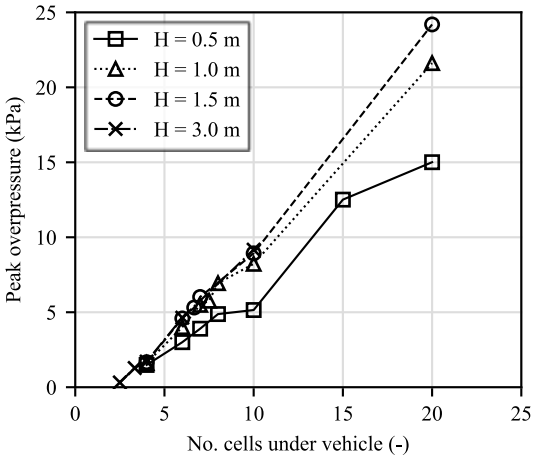

b) Peak impulse vs No. cells under vehicle

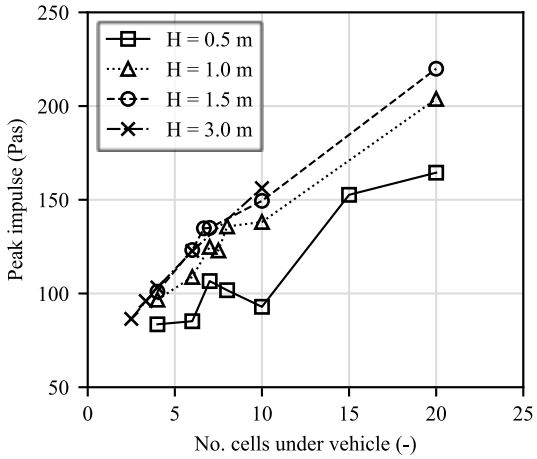

Figure 37. Relationship between the number of cells under the vehicle and a) the peak overpressure and b) peak impulse at monitor point BOT_14 within Campaign III.

4.5 Stage I: Campaign IV

The peak overpressure at a monitor point located at a distance of 1.0 m from the modelled vehicle (monitor point MP_9_9) is presented in Figure 38 for different grid resolutions and different values of the initial fluctuating velocity, *u'*. The grid resolution is expressed in terms of the number of cells along the distance between the vehicle and the ground, N_{veh}, as well as in terms of the grid cell size. The results show a nearly linear relationship between the peak overpressure and the cell count for all considered values of initial fluctuating velocity. This indicates a strong grid dependency regardless of initial turbulence conditions, whereby smaller grid cell sizes produce greater values of overpressure. It appears that further refinement of the grid is not likely to lead to convergence (although smaller cell sizes would be impractical).

Moreover, Figure 38 shows a significant difference in overpressure between the configuration with the default value (*u'* = 60 m/s) and the other two cases. In contrast, the difference in results between the cases with *u'* = 1.0 m/s and *u'* = 0.1 m/s is relatively small. The results suggest that choosing an arbitrary value of initial fluctuating velocity within the interval [0.1 m/s, 1.0 m/s] is not likely to have a significant impact on the results. Indeed, the uncertainties related to the grid cell size may have a more critical effect on the results. Rather than figuring out an exact value of initial turbulence velocity for a given scenario (something which would be impractical), it is more important to capture the right order of magnitude. Based on these results, a value of *u'* = 1.0 m/s was therefore judged to lead to conservative but realistic estimates.

a) Peak overpressure vs No. cells under car

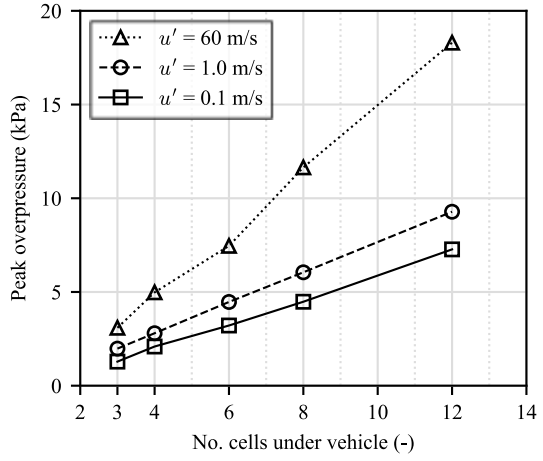

b) Peak overpressure vs grid cell size

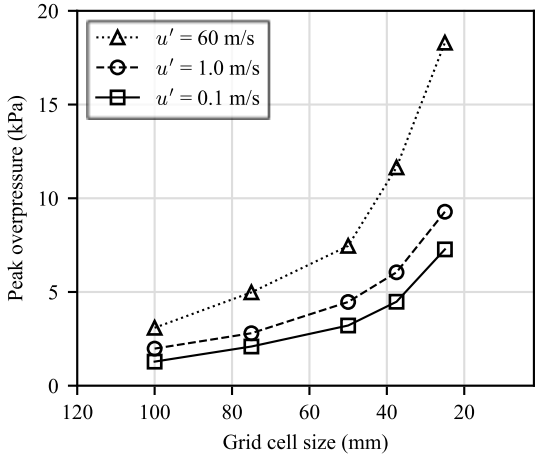

Figure 38. Peak overpressure at monitor point MP_9_9 for different grid resolutions and initial fluctuating velocity, u'. Campaign IV.

Figure 39 gives the peak impulse as a function of grid resolution and initial fluctuating velocity. Just as for the peak overpressure, using greater values of initial turbulent velocity yields greater peak impulse. However, the increase in peak impulse between the configurations with *u'* = 0.1 m/s and *u'* = 1.0 m/s is similar to the increase in peak impulse between the configurations with *u'* = 1.0 m/s and *u'* = 60.0 m/s. This contrasts with the results regarding peak overpressure, for which a clearly greater enhancement is observed for the configurations with *u'* = 60.0 m/s compared to the configurations with the other two values.

a) Peak impulse vs No. cells under car

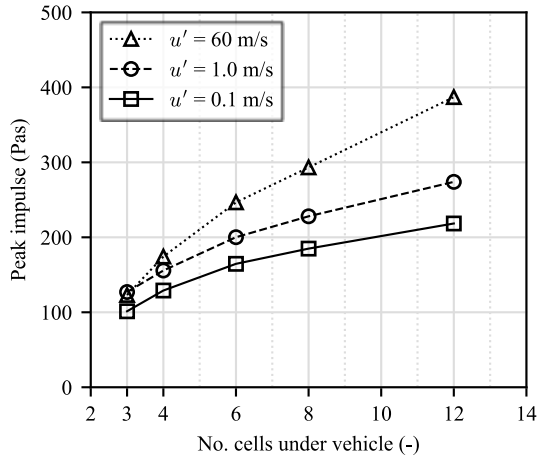

b) Peak impulse vs grid cell size

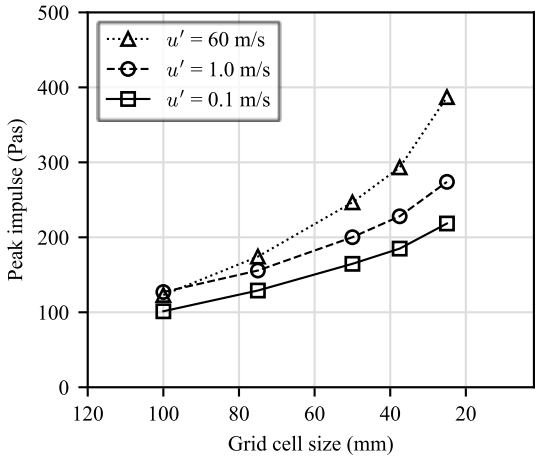

Figure 39. Peak impulse at monitor point MP_9_9 for Campaign IV.

When the influence of the initial turbulence is studied in relative terms, as shown in Figure 40, it is observed that the enhancement of peak pressure and peak impulse due to the increase of the initial turbulence velocity subsides as the initial turbulence velocity approaches the default value. In Figure 40a), the relative difference in peak overpressure between the configurations with u' = 0.1 m/s and u' = 1.0 m/s is about 1.4, while the difference between the configurations with u' = 0.1 m/s and u' = 60 m/s is in average 2.5. That is, an increase of the initial fluctuating velocity with a factor of 10 from a small value produced an increase with a factor 1.4, while an increase in initial fluctuating velocity with a factor of 600 led to a pressure increase with a factor of 2.5.

The increase in peak impulse due to the increase of the initial fluctuating velocity is in general smaller than the corresponding increase of peak overpressure, based on comparison between Figure 40a) and Figure 40b). In average, the relative difference between the configurations with u' = 0.1 m/s and u' = 1.0 m/s is about 1.2, while the difference between the configurations with u' = 0.1 m/s and u' = 60 m/a is in average 1.5. However, the increase between u' = 0.1 m/s and u' = 1.0 m/s remains constant regardless of grid refinement, while it increased for a refined grid when u' is set to 60.0 m/s. This indicates that the initial increase in turbulent velocity has a relatively larger effect, but the impact decreases for greater values of turbulent velocity. However, in absolute terms, the increase of pressure and impulse in the initial interval is still smaller than the uncertainty related to the grid dependency.

a) Peak overpressure

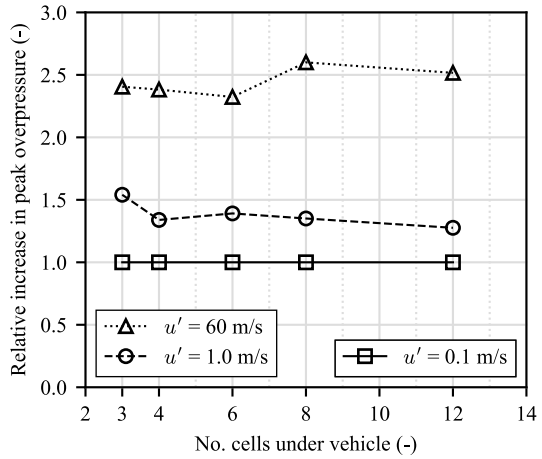

b) Peak impulse

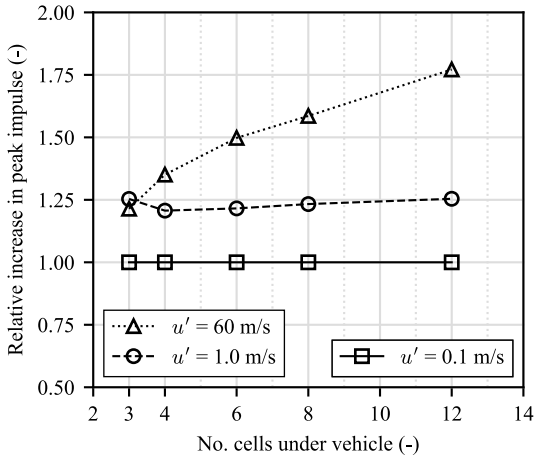

Figure 40. Influence of initial fluctuating velocity, u', on the peak overpressure at monitor point MP_9_9 for Campaign IV. The results were normalized with regard to u' = 0.1 m/s.

4.6 Stage II: Campaign V

Figure 41 shows the flame speed as a function of the distance from the ignition point for configuration 1, in which the distance between confining plates, H, is equal to 0.3 m. The results are given for different numbers of grid cells along the distance between plates, N_H. The lines represent the numerical results, while the scattered triangles correspond to the experimental values. It can be seen that $N_H = 3$ and $N_H = 6$ yielded values of flame speed similar to the experimental results. In contrast, the flame speed was overpredicted for greater values of N_H (i.e., smaller cell size). A similar trend was observed for other values of H (not shown here). The case with $H = 0.3$ m is of particular interest because this is the same dimension assumed for the region under the vehicles in (Lozano, 2023; Makarov et al., 2009). The drop of flame speed at approximately 2.1 m for all cases was due to deacceleration of the flame as it exited the congested area.

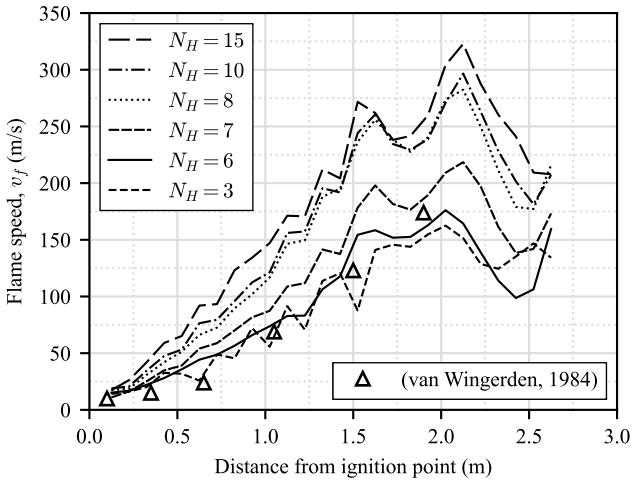

Figure 41. Comparison between results with FLACS-CFD and the experiment in (van Wingerden, 1984): Flame speed vs distance for different values of grid cell size and H = 0.3 m.

It should be noted that the flame speed is not a standard output produced directly by FLACS-CFD. Instead, it was calculated based on other output parameters. First, the arrival time of the flame front at two consecutive monitor points was calculated, which was then used to find the travel time between the points. The arrival time of the flame was determined based on the profile of temperature over time as

the time at which the temperature at the monitor point reached a value of 1500 K. The flame speed was then computed from the travel time and the known distance between the points.

Figure 42 gives the peak overpressure as a function of distance for all three configurations. The results are given for different values of distance between confining planes, H, and cell count, N_H. The peak overpressure predicted by FLACS-CFD clearly increased with increasing N_H for all values of H. In general, it appears that the models with cell count between $N_H = 3$ and $N_H = 6$ produce reasonable predictions for all the studied values of H. A trend towards moderate overprediction of the overpressure was observed for $N_H = 6$, whereas $N_H = 3$ led to results that are similar to or lower than the experimental measurements. Furthermore, the hypothesis that the grid resolution should be based on the cell count along the main distance of confinement (which was also observed in Campaign III) seems to hold for different values of the distance between confining planes.

a) Configuration 1 ($H = 0.3$ m)

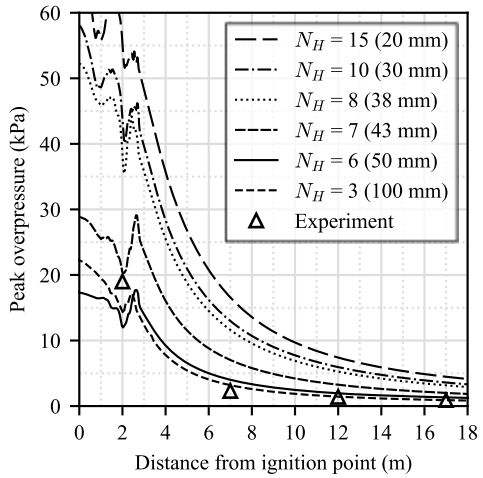

b) Configuration 2 ($H = 1.0$ m)

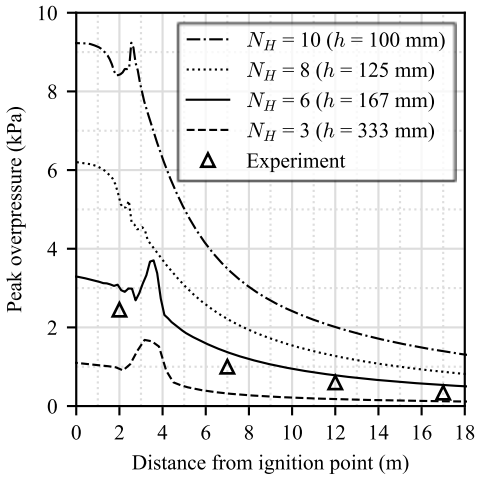

c) Configuration 3 ($H = 0.12$ m)

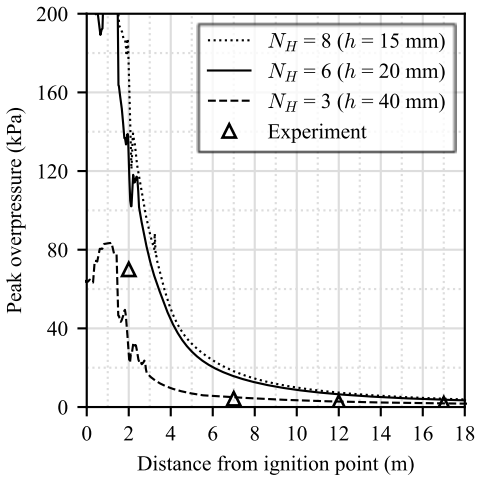

Figure 42. Comparison between FLACS-CFD and Experiment I (van Wingerden, 1984): Peak overpressure vs distance for different values of grid cell size and distance between plates, H.

Therefore, the comparison with the experiment in (van Wingerden, 1984) suggests that choosing a cell count between $N_H = 3$ and $N_H = 6$ in the main dimension of confinement would lead to reasonable results both inside and outside the confined region. For this reason, value of $N_H = 3$ and $N_H = 6$ were used in the simulations of the experiment by (van Wingerden, 1989) in Campaign VI.

It should be noted that the simulations described here were performed with the initial fluctuating velocity set to u' = 1 m/s. This value is considered a reasonable upper limit to represent the turbulence conditions right before ignition in the experiments, in which mixing of the flammable gas and air was achieved with fans. However, to test the sensitivity of this parameter, simulations with u' = 60 m/s and u' = 0.1 m/s were also carried out for configuration 1.

The influence of the initial fluctuating velocity is illustrated in Figure 43. In general, greater values of initial fluctuating velocity produced greater overpressure and impulse. However, simulations with u' = 1.0 m/s and u' = 0.1 m/s yielded comparable results. The greatest error between results with these two initial velocities was 18 % for the peak overpressure and 4 % regarding peak impulse. Furthermore, the results are nearly equal for $N_H \leq 6$. On the other hand, simulations with the default value of u' (60 m/s) significantly overpredicted the overpressure for $N_H \geq 8$, although it produced lower overpressure for $N_H = 3$. The greatest error between results with u' = 1.0 m/s and u' = 60 m/s was 66 % for the peak overpressure and 30 % for the peak impulse. In general, peak impulse appears to be less sensitive to the initial turbulence conditions.

a) Peak overpressure vs No. cells under car

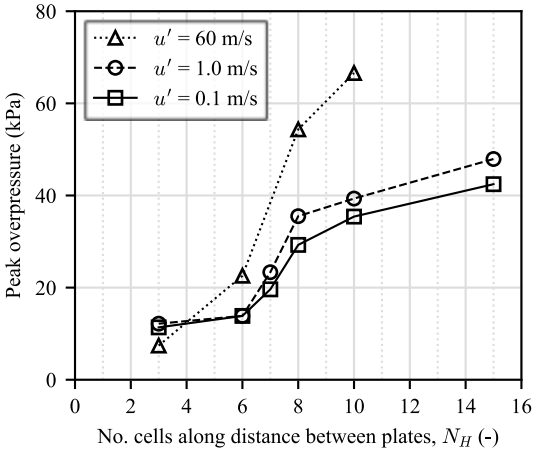

b) Peak impulse vs No. cells under car

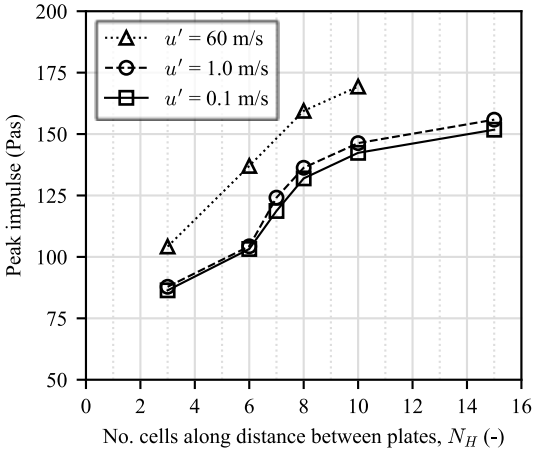

Figure 43. Influence of the initial fluctuating velocity in Configuration 1 (H = 0.3 m) in Campaign V. The results are collected from monitor point MP_10_6.

4.7 Stage II: Campaign VI

The results from Campaign V indicated that for explosion scenarios in which expansion occurs predominantly in two dimensions, the main dimension of confinement should be discretized with 3 to 6 cells. Thus, in Campaign VI, values of $N_H = 3$ and $N_H = 6$ were used in the simulations of the experiment by (van Wingerden, 1989). As the distance between the confinement plates in (van Wingerden, 1989) was 0.3 m, the two tested grid cell sizes were 0.3 m/3 = 100 mm and 0.3 m/6 = 50 mm. Figure 44 and Figure 45 show the results in the form of flame speed as a function of the distance from the ignition point for ethylene and propane, respectively. It should be noted that the vertical tubes in the experiment by (van Wingerden, 1989) lead to wrinkling and folding of the flame front in the regions between rows of tubes, which causes large variation of the flame speed at given radial distance from the ignition point. The numerical results presented in Figure 49 and Figure 50 are average values calculated from the results at several points located at the same radial distance from the ignition point. However, large deviations from the average values were observed in the zones between rows of tubes.

The experimental results lie between the numerical results with $N_H = 3$ and $N_H = 6$. The models with $N_H = 3$ underpredicted the flame speed slightly, whereas $N_H = 6$ led to overprediction. That is, the recommended interval for the cell count in the direction of confinement appears to provide a reasonable

lower and upper limit for the prediction of flame speed. Results with N_H = 3 are closer to the experimental values. It is likely than using greater values of N_H would produce even greater flame speed, which would make greater values of N_H irrelevant. An interesting observation is that the degree of overprediction with N_H = 6 appears to be similar for both types of gases.

Finally, it can be observed in Figure 44 and Figure 45 that varying the initial fluctuation velocity between *u'* = 1.0 m/s and *u'* = 0.1 m/s has negligible impact on the resulting flame speed.

In general, the results from this campaign agree with the conclusions reached in Campaign V.

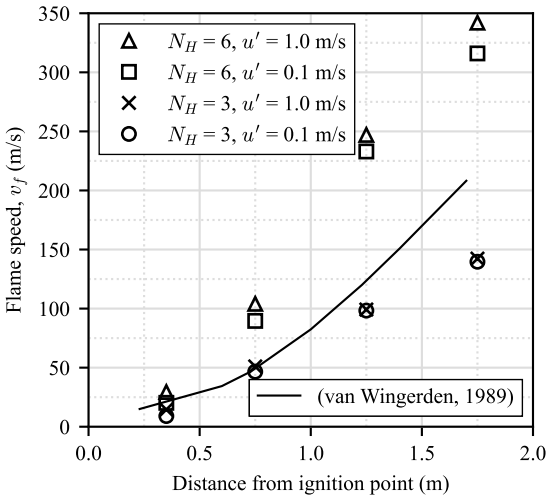

Figure 44. Comparison between results with FLACS-CFD and the experiment in (van Wingerden, 1989): Flame speed vs distance for different values of grid size and ethylene-air mixture.

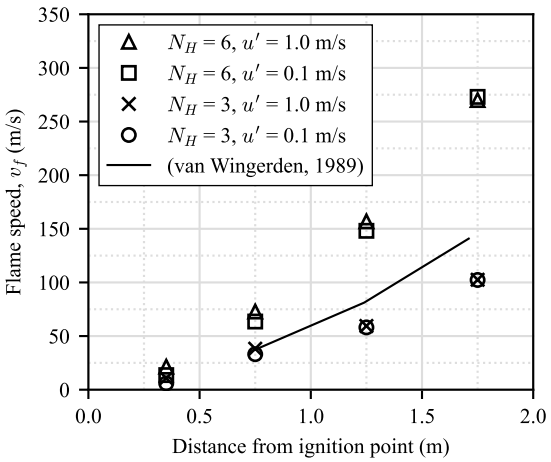

Figure 45. Comparison between results with FLACS-CFD and the experiment in (van Wingerden, 1989): Flame speed vs distance for different values of grid size and propane-air mixture.

5 Discussion

In Campaign I, grid dependency in FLACS-CFD was evaluated for two configurations with the same mixture composition and the same gas cloud shape. The only difference between the two configurations was that in one of them the cloud was completely unobstructed, while in the other one there was a vehicle centrally placed inside the cloud. For both configurations, a strong grid dependency was observed: refining the grid resulted in an increase in both peak overpressure and peak impulse. The peak impulse was shown to be less sensitivity to the grid resolution than the overpressure. This means that a conventional grid convergence analysis is not sufficient to make a choice of grid resolution for this type of model. This campaign also provided insight regarding the level of resolution necessary to properly resolve the flow in the confined region under the vehicle. The results showed that the enhancement on the peak overpressure and impulse due to confinement under the vehicle was only captured when the space under the car was discretized with at least three cells.

In Campaign III, simulations of explosions of a propane-air cloud engulfing a single vehicle were carried out. Grid sensitivity analysis in conjunction with the effects of the cloud height was investigated in this campaign. The height of the gas cloud was varied, while keeping the horizontal area of the cloud constant. This campaign evaluated the recommendations on the user's manual (Gexcon AS, 2022) for the choice of grid cell size based on the smallest dimension of the cloud. The results show that choosing the cell size based on the height of the cloud (which was the smallest dimension of the cloud for all cases) resulted in unrealistic results whereby the scenarios with the least gas volume (smallest height) produced the greatest peak overpressure. This contradicts theory as, for the geometrical conditions of this study, similar values of overpressure are expected inside the confined volume regardless of the cloud size outside the confined region, while greater overpressure is expected outside the vehicle for scenarios with larger gas volume. This counterintuitive result is a consequence of the approach for selecting grid size: by defining the grid size as a function of the cloud dimension, the needed grid size would necessarily be smaller as the gas cloud size decreases, and smaller grid sizes lead to greater values of overpressure. The main conclusion from this campaign is that basing the grid cell size on the smallest dimension of the cloud is not appropriate for this type of scenario. Instead, the results showed that the grid cell size may be based on the number of cells along the main dimension of confinement.

The question remains whether the height of the confined region under the vehicle should be regarded as the smallest dimension of the cloud. That is, whether the requirement of at least 15 cells should be applied to this region. For the geometry of the vehicles assumed in this work, that would mean that the maximum cell size in Campaign III should be $500/15 \approx 33$ mm, while the maximum cell size in Campaign IV should be $300/15 = 20$ mm. However, the results presented across all campaigns indicate that this cell size is likely to lead to significant overprediction of both the overpressure and impulse. Furthermore, this approach would lead to extremely large and impractical models in many projects. Depending on the geometry of the vehicle on a given project, this may also produce cells that are smaller than the minimum allowed cell size.

A possible solution would be to treat the confined region under the vehicle as a *vent*. For explosion scenarios with vents, the recommendation in the user's manual for v.22 (Gexcon AS, 2022) is to use a minimum of 3 cells across the vent. In the manual for v.21 (Gexcon AS, 2021) there is a requirement of at least 7 cells across *significant vents*. Using these two values, a tentative interval for cell count along the distance between vehicles and ground can be proposed: [3, 7].

Adopting 6 cells under the vehicle, for example, would give a cell size of $500/6 \approx 83$ mm for the scenarios in Campaign III, which in turns imply that the total gas cloud would be divided into 6, 12, 18 and 36 cells for a cloud height of 0.5, 1.0, 1.5, and 3.0 m, respectively. That is, the guideline to use at least 15 cells would not be fulfilled in some cases. Nonetheless, this may be an acceptable approach for "pancake" clouds, in which the height of the cloud is considerably smaller than the other dimensions.

This approach would result in very similar results inside the confined region (and in the neighbouring area) regardless of the size of the cloud outside the confined volume. The effects of this approach for choosing the grid size on the far-field results remains to be studied.

For highly congested scenarios, in which multiple repetitive small obstacles are present, it appears that the recommendation based on the cloud size may produce reasonable results. This was investigated in Campaign II. However, in the evaluated scenarios, the size of the gas cloud is the same as the size of the congested region, which means that it is possible that discretization should be based on the size of the congested region. The scenarios in this campaign were the only one that showed signs of convergence for a given interval of grid resolutions among all campaigns presented in this report. This is perhaps not surprising, since the code was originally intended to solve this kind of environment with the PDR approach. Thus, the sub-grid models are better suited for these conditions. However, upon further refinement, the model seemed to break down and lead to significantly larger values of overpressure. A user must then be careful to identify when the results start to diverge. In general, it was observed that the peak impulse was less sensitive to the variation of the grid resolution.

Campaign IV investigated the effects of the initial turbulence conditions in combination with the grid sensitivity for scenarios consisting of a vehicle engulfed by a propane-air cloud. Once again, no sign of grid convergence could be discerned. Instead, refining the grid resolution consistently led to an increase in both the peak overpressure and the peak impulse. Increasing the initial turbulent velocity was observed to have an enhancing effect on the resulting overpressure and impulse. Increasing the initial fluctuating velocity from 0.1 m/s to 1.0 m/s (factor 10), increased the peak overpressure with a factor of 1.4, averaged across all grid resolutions. Increasing the initial fluctuating velocity from 0.1 m/s to 60 m/s (factor 600), increased the peak overpressure with a factor of 2.5. This indicates that the influence of the initial turbulence conditions gradually decreases for increasing values of initial turbulence velocity. However, the results show that the uncertainty related to the choice of grid cell size is greater than the effect of the initial turbulence conditions. Therefore, it is more important to get the right order of magnitude of initial turbulence velocity, rather than focusing on finding an exact value. A value of 1.0 m/s is believed to be reasonable maximum limit for the conditions in a traffic environment (representative of a wind speed of 1 m/s and relative turbulence intensity of 10 %).

In general, the main outcome from Stage I was that significant grid dependency is present in simulations of gas explosions in a traffic environment with FLACS-CFD. The peak impulse was found to be less sensitive to the variation of the grid resolution. Furthermore, the user's guidelines are not sufficient to make a consistent and appropriate choice of grid cell size. For that reason, calibration against relevant experimental work is required in order to find an appropriate grid cell size for the scenario of interest. This was the main objective of Stage II, in which comparison between numerical simulations with FLACS-CFD and two experimental campaigns were carried out. The evaluated experiments were selected from the literature. The main feature of the two selected experiments is that the combustion should take place in a congested region between two parallel confining planes. That is, the flow was predominantly two-dimensional, which is an approximation of the flow characteristics in the region under the vehicles.

In Campaign V, simulations of the experiment by (van Wingerden, 1984) were performed. By comparing the flame speed inside the congested region and the peak overpressure outside the congested region, it was shown that discretizing the main direction of confinement (distance between the confining plates) with 3 to 6 cells yield results comparable with the experimental measurements. Choosing 3 cells led to a slight underprediction, while 6 cells produced reasonably conservative results. This campaign also showed that the difference in results for an initial turbulence velocity of 0.1 m/s and 1 m/s is negligible for the recommended range of cell count (3 to 6 cells), though larger variation was observed when comparing results from models with initial turbulence velocity set to 60 m/s. The recommended range is in agreement with the initial tentative conclusion from the results in Campaign III: that the space under the car could be treated as a vent, meaning that between 3 and 7 cells should be used to discretize

this region. Furthermore, a discretization with 3 to 6 cells has also been used by other authors (Makarov et al., 2009; Middha, 2010).

In Campaign VI, the experiment by (van Wingerden, 1989) was simulated using a cell count based on the conclusions from campaign V, that is, 3 and 6 cells along the distance between confining plates. In general, the results from this campaign agreed with the conclusions reached in Campaign V. The results show that the model slightly underpredicts the flame speed when using 3 cells along the distance between confining plates, while it leads to overprediction with 6 cells. That is, using between 3 and 6 provides a confidence zone within which the experimental measurements lie. Using 6 cells will lead to conservative results. In this campaign, little difference between models with an initial turbulence velocity of 0.1 m/s and 1 m/s was observed.

6 Conclusions

In this report, an extensive numerical study of the grid sensitivity of gas explosion simulations in a traffic environment with the software FLACS-CFD was carried out. The work was divided into six campaigns, grouped into two stages. Several scenarios were analysed within each campaign.

The results from Stage I showed strong grid dependency for cases consisting of a vehicle engulfed by a gas cloud. Refining the grid consistently resulted in greater peak overpressure and peak impulse. The peak impulse appears to be less sensitive to the variation of the grid cell size. This means that a conventional grid convergence analysis is not sufficient to make a choice of grid resolution for this type of model.

Furthermore, the results suggest that for this type of cases, in which ignition and combustion take place in a volume with two-dimensional confinement, it is not suitable to define the grid size solely as a function of the cloud size outside the confined region. The geometrical boundaries of the confined region (region under the vehicle) should also be taken into consideration when choosing a grid size. In fact, for "pancake" clouds (the height is considerably smaller than the other dimensions) in situations where a vehicle is the source of congestion, it may be more appropriate to choose a grid cell size based on recommendations for discretizing the region under the vehicle. This appears to be valid at least for cases in which the results inside a region with two-dimensional confinement (and in the neighbouring area) are of interest.

To assist the users in the choice of grid cell size for simulations involving two-dimensional confinement, a comparison between numerical analyses and experimental results (from two gas explosion experiments available in the literature) was carried out in Stage II. The results indicate that for situations in which the flow is confined by two parallel planes, it may be suitable to discretize the direction of confinement (i.e., the distance between the confining planes) with 3 to 6 cells. Using 6 cells is likely to produce moderately conservative results. The cell size determined with the recommended cell count should then be used in the entire confined region and outside the region where external explosion is possible. Therefore, for a scenario in which a vehicle is the source of confinement, the cell size can be determined by dividing the distance between the underside of the vehicle and the ground into 3 to 6 elements. The resulting cells size is used under the vehicle and outside the vehicle in the domain where external explosion is possible.

This study was done on FLACS-CFD version 22. Newer versions of the software may have a different convergence behaviour. Furthermore, the flammable mixture was introduced in the models as an equivalent gas cloud with regular shape and stochiometric concentration. The grid dependency of scenarios with dispersed clouds with variable concentration remains to be investigated.

References

Arntzen, B. J. (1998). *Modelling of turbulence and combustion for simulation of gas explosions in complex geometries* [Ph.D. Thesis]. NTNU: Norwegian University of Science and Technology.

Both, A.-L., Atanga, G., & Hisken, H. (2019). CFD modelling of gas explosions: Optimising sub-grid model parameters. *Journal of Loss Prevention in the Process Industries*, *60*, 159–173. https://doi.org/10.1016/j.jlp.2019.04.008

Bradley, D. (1978). The venting of gaseous explosions in spherical vessels. II - Theory and experiment. *Combustion and Flame*, *32*.

Bubbico, R., Ferrari, C., & Mazzarotta, B. (2000). Risk analysis of LPG transport by road and rail. *Journal of Loss Prevention in the Process Industries*, *13*(1), 27–31. https://doi.org/10.1016/S0950-4230(99)00057-1

Casal, J. (2017). *Evaluation of the effects and consequences of major accidents in industrial plants* (2nd ed.). Elsevier.

Center for Chemical Process Safety. (2010). *Guidelines for vapor cloud explosion, pressure vessel burst, BLEVE, and flash fire hazards* (2nd ed.). John Wiley & Sons, Inc. https://doi.org/10.1002/9780470640449

Eurostat. (n.d.). *Road freight transport of dangerous goods by type of dangerous goods and territorial coverage* [Dataset]. Retrieved June 8, 2023, from https://ec.europa.eu/eurostat/databrowser/view/road_go_ta_dg/default/table?lang=en

Gexcon AS. (2020, September 30). *FLACS v20.1 User's Manual*.

Gexcon AS. (2021, December 21). *FLACS v21.3 User's Manual*.

Gexcon AS. (2022, April 27). *FLACS-CFD v22.1 User's Manual*.

Hansen, O. R., Hinze, P., Engel, D., & Davis, S. (2010). Using computational fluid dynamics (CFD) for blast wave predictions. *Journal of Loss Prevention in the Process Industries*, *23*(6), 885–906. https://doi.org/10.1016/j.jlp.2010.07.005

Hjertager, B., Fuhre, K., & Bjørkhaug, M. (1988). *Spherical gas explosion experiments in a high-density obstructed 27 m3 corner*. Chr. Michelsen institute.

Hjertager, B. H. (1984). *Computer simulation of turbulent reactive gas dynamics*. *5*(4), 211–236. https://doi.org/10.4173/mic.1984.4.3

Hjertager, B. H. (1993). Computer modelling of turbulent gas explosions in complex 2D and 3D geometries. *Journal of Hazardous Materials*, *34*(2), 173–197. https://doi.org/10.1016/0304-3894(93)85004-X

Hjertager, B., Sæter, O., & Solberg, T. (1996). *Numerical modelling of gas explosions—A review*.

Hu, Q., Qian, X., Shen, X., Zhang, Q., Ma, C., Pang, L., Liang, Y., Feng, H., & Yuan, M. (2022). Investigations on vapor cloud explosion hazards and critical safe reserves of LPG tanks. *Journal of Loss Prevention in the Process Industries*, *80*, 104904. https://doi.org/10.1016/j.jlp.2022.104904

Johansson, M. (2012). *Luftstötvåg (Blast waves in air)* (MSB448).

Launder, B., & Spalding, D. B. (1974). The numerical computation of turbulent flow computer methods. *Computer Methods in Applied Mechanics and Engineering*, *3*, 269–289. https://doi.org/10.1016/0045-7825(74)90029-2

Lea, C. J., & Ledin, H. S. (2002). *A Review of the state-of-the-art in gas explosion modelling* (HSE HSL/2002/02; p. 180). Health and Safety Laboratory.

Lozano, F. (2023). *Explosions in urban environments: Modelling of gas explosions and risk of premature shear failure in reinforced concrete structures* [Lic. Thesis]. Chalmers University of Technology.

Makarov, D., Verbecke, F., Molkov, V., Roe, O., Skotenne, M., Kotchourko, A., Lelyakin, A., Yanez, J., Hansen, O., Middha, P., Ledin, S., Baraldi, D., Heitsch, M., Efimenko, A., & Gavrikov, A. (2009). An inter-comparison exercise on CFD model capabilities to predict a hydrogen explosion in a simulated vehicle refuelling environment. *International Journal of Hydrogen Energy*, *34*(6), 2800–2814. https://doi.org/10.1016/j.ijhydene.2008.12.067

Middha, P. (2010). *Development, use, and validation of the CFD tool FLACS for hydrogen safety studies* [Ph.D. Thesis, University of Bergen]. https://doi.org/10.13140/RG.2.2.21729.71520

Middha, P., & Hansen, O. R. (2009a). CFD simulation study to investigate the risk from hydrogen vehicles in tunnels. *International Journal of Hydrogen Energy*, *34*(14), 5875–5886. https://doi.org/10.1016/j.ijhydene.2009.02.004

Middha, P., & Hansen, O. R. (2009b). Using computational fluid dynamics as a tool for hydrogen safety studies. *Journal of Loss Prevention in the Process Industries*, *22*(3), 295–302. https://doi.org/10.1016/j.jlp.2008.10.006

Mishra, S., & Mishra, K. B. (2021). Numerical study of large-scale LNG vapour cloud explosion in an unconfined space. *Process Safety and Environmental Protection*, *149*, 967–976. https://doi.org/10.1016/j.psep.2021.03.034

Momferatos, G., Giannissi, S. G., Tolias, I. C., Venetsanos, A. G., Vlyssides, A., & Markatos, N. (2022). Vapor cloud explosions in various types of confined environments: CFD analysis and model validation. *Journal of Loss Prevention in the Process Industries*, *75*, 104681. https://doi.org/10.1016/j.jlp.2021.104681

Patankar, S. V., & Spalding, D. B. (1974). A Calculation procedure for the transient and steady-state behaviour of shell-and-tube heat exchangers. In *N.H. Afgan and E.V. Schhinder (eds.), Heat Exchangers: Design and Theory Sourcebook* (pp. 155–176). McGraw-Hill.

Pedersen, H., & Middha, P. (2012). Modelling of vented gas explosions in the CFD tool FLACS. *Chemical Engineering Transactions*, *26*. https://doi.org/10.3303/CET1226060

Puttock, J., Walter, F., Chakraborty, D., Raghunath, S., & Sathiah, P. (2022). Numerical simulations of gas explosion using Porosity Distributed Resistance approach Part −1: Validation against small-scale experiments. *Journal of Loss Prevention in the Process Industries*, *75*, 104659. https://doi.org/10.1016/j.jlp.2021.104659

Sha, W. T., & Launder, B. E. (1979). *A model for turbulent momentum and heat transport in large rod bundles* (Report ANL-77-73). Argonne National Laboratory.

Sha, W. T., Yang, C. I., Kao, T. T., & Cho, S. M. (1982). Multidimensional numerical modeling of heat exchangers. *Journal of Heat Transfer*, *104*(3), 417–425. https://doi.org/10.1115/1.3245109

Shi, Y., Xie, C., Li, Z., & Ding, Y. (2021). A quantitative correlation of evaluating the flame speed for the BST method in vapor cloud explosions. *Journal of Loss Prevention in the Process Industries*, *73*, 104622. https://doi.org/10.1016/j.jlp.2021.104622

Skjold, T., Hisken, H., Lakshmipathy, S., Atanga, G., Carcassi, M., Schiavetti, M., Stewart, J., Newton, A., Hoyes, J. R., TOLIAS, I., Venetsanos, A., Hansen, O., Geng, J., Huser, A., Helland, S., Jambut, R., Ren, K., Kotchourko, A., Jordan, T., & Bauwens, C. R. (2018). Blind-prediction: Estimating the consequences of vented hydrogen deflagrations for homogeneous mixtures in 20-foot ISO containers. *International Journal of Hydrogen Energy*, *44*. https://doi.org/10.1016/j.ijhydene.2018.06.191

Skjold, T., Pedersen, H. H., Narasimhamurthy, V. D., Lakshmipathy, S., Pesch, L., Atanga, G., Folusiak, M., Bernard, L., Siccama, D., & Storvik, I. E. (2014). *Pragmatic modelling of industrial explosions in complex geometries: Review of the state-of-the-art and prospects for the future. 1*, 70–74.

Tolias, I. C., Stewart, J. R., Newton, A., Keenan, J., Makarov, D., Hoyes, J. R., Molkov, V., & Venetsanos, A. G. (2018). Numerical simulations of vented hydrogen deflagration in a medium-

scale enclosure. *Journal of Loss Prevention in the Process Industries*, *52*, 125–139. https://doi.org/10.1016/j.jlp.2017.10.014

Van den Schoor, F., Middha, P., & Van den Bulck, E. (2013). Risk analysis of LPG (liquefied petroleum gas) vehicles in enclosed car parks. *Fire Safety Journal*, *57*, 58–68. https://doi.org/10.1016/j.firesaf.2012.10.026

van Wingerden, C. J. M. (1984). *Experimental study of the influence of obstacles and partial confinement on flame propagation, Part II* (EUR 9541 EN/II; Commission of the European Communities for Nuclear Science and Technology). TNO Prins Maurits Laboratory.

van Wingerden, C. J. M. (1989). Experimental investigation into the strength of blast waves generated by vapor cloud explosions in congested areas. *6th Int. Symp. on Loss Prevention and Safety Promotion in the Process Industries*.

Vyazmina, E., & Jallais, S. (2016). Validation and recommendations for FLACS CFD and engineering approaches to model hydrogen vented explosions: Effects of concentration, obstruction vent area and ignition position. *International Journal of Hydrogen Energy*, *41*. https://doi.org/10.1016/j.ijhydene.2016.05.189

Wang, S., Li, Z., Fang, Q., Yan, H., & Liu, Y. (2022). Numerical simulation of overpressure loads generated by gas explosions in utility tunnels. *Process Safety and Environmental Protection*, *161*, 100–117. https://doi.org/10.1016/j.psep.2022.03.014

DEPARTMENT OF ARCHITECTURE AND CIVIL ENGINEERING
CHALMERS UNIVERSITY OF TECHNOLOGY
Gothenburg, Sweden
www.chalmers.se

CHALMERS
UNIVERSITY OF TECHNOLOGY